Development and Application of Monte Carlo Neutronics Methodologies for Safety Studies of Current Operating Reactors

Descrittori

Tipologia del documento: Rapporto Tecnico

Collocazione contrattuale: Accordo di Programma ENEA-MSE su sicurezza nucleare e reattori di IV generazione

Argomenti trattati: Metodi Monte Carlo
Neutronica
Reattori Nucleari Evolutivi
Calcoli di Schermaggio
Tecniche Riduzione della Varianza

Sommario

This report deals with radiation transport calculations supporting safety analysis of nuclear reactors. The calculations employ Monte Carlo with the MCNP code and use the DSA variance reduction methodology. The first part of the report contains an analysis of ex-core responses, in particular pressure vessel damage, in a Gen-III PWR. Results from two approaches are compared. The first approach involves a decoupling of the problem. An analog simulation of the eigenvalue problem is performed and a fission source is created. This source is then used in a fixed source calculation with variance reduction parameters generated with the DSA. The second approach calculates the ex-core responses within the eigenvalue problem, again employing the DSA. The second part of the report deals with the PCA-Replica benchmark (SINBAD archive NEA-1517/93) concerning integral experiments performed at the NESTOR research reactor (Winfrith, UK). A fission plate irradiates a mock-up reproducing key materials for LWRs. The results are neutron spectra and dosimeter responses. Various nuclear data libraries are compared. The results show a satisfactory agreement between calculation and experiment.

Note

The authors of this report are:
K.W. Burn, P. Console Camprini

Copia n.			In carico a:			
2			NOME			
			FIRMA			
1			NOME			
			FIRMA			
0	EMISSIONE	08-11-2017	NOME	K. W. Burn	F. Padoani	F. Rocchi
			FIRMA			
REV.	DESCRIZIONE	DATA		REDAZIONE	CONVALIDA	APPROVAZIONE

Table of Contents

1. Introduction

Within the framework of safety analysis of nuclear systems, several modelling tools and numerical methodologies are utilized in order to represent possible scenarios and find out in detail the capacity of response of the facility - facing incidental or accidental conditions.

These evaluations are relevant during both the design and the licensing process and are a subject of interest for technical support organizations (TSO) and nuclear safety agencies, as well as research institutions.

Regarding the specific context of the analysis, a typical objective is the description of a neutron or photon source within a certain domain. The main aim is the definition of the consequent particle migration and the transport throughout the system.

The Monte Carlo method is employed in this field, being a powerful mathematical approach which allows a detailed description of the domain in question, together with a continuous-energy description of particle tracks in the phase space.

The history of each particle is reproduced, according to nuclear reactions defined by probability laws and sampling among all possible outcomes. Many such histories are simulated with this procedure until adequate confidence intervals on chosen responses are spawned. The neutron or photon flux is obtained, as well as related physical quantities, within detectors or control volumes of interest. Both fluxes and reaction rates such as dose and energy deposition may be required.

By contrast, the simulation of systems in which a consistent particle production is related to the intrinsic particle flux – namely multiplicative systems – forms a particular class of problems. In fact, simulation of nuclear fuel (composed of fissionable nuclides) belongs to this category. Firstly, it is necessary to characterize the source inherent to the medium and then it is possible to represent the effects of such a source in terms of each response of interest.

Sometimes the portions of phase space characterized by the requested response cannot be easily reached by the particles which populate the samples. In these cases, the targets are “far” from the particle generation points and the contribution to statistics is insufficient or – worse – almost absent even for a large number of histories simulated. The reason is always physical: it means that the particles do not easily find the path to travel deeply into the system to reach the desired target. This class of situations is usually called “deep penetration”.

Since physical features of the system do not allow to easily reach a particular portion of it, it is necessary to force the simulation to collect more particle histories that provide contributions. Various techniques are then devoted to the “variance reduction” of the simulation, increasing the quality of the statistics for a given response, reducing the associated variance. More interesting paths are stressed and populated with respect to less interesting ones. Of course such a distortion of the initial system is not physical and corrections are employed to take into account this artificial modification, keeping the average values constant

The present study is focused on the lifetime extension of currently operating nuclear power reactors and particularly on the estimation of the dose delivered to the reactor pressure vessel of a Gen-III PWR by both the neutron radiation and the gamma field. The continuous irradiation of structural materials causes atom displacement (dpa) in the medium and impacts the mechanical integrity. Particular attention is dedicated to the vessel reliability during operation [1].

The physical quantities used to evaluate the radiation impact for these purposes are neutron dpa and gamma dpa, or neutron fluence (energy above 1 MeV) and gamma kerma. Monte Carlo methods are suitable for the estimation of neutron and gamma contributions to dpa, since accurate responses are requested at particular points of the system – namely ex-core locations.

For some years, ENEA has been involved in the the development and implementation of variance reduction techniques in Monte Carlo simulations of radiation transport [2]. Normally, variance reduction is properly employed for problems in which a fixed source is defined. Histories are produced according to source specification together with suitable distortion biasing toward the locations of the region interested by responses. Instead more recently the techniques have been extended to eigenvalue problems [3].

The standard approach creates a source related to a multiplicative system: particle histories are simulated according to nature in analog mode. The source produced in this way is employed to generate particles and transport them toward the detectors – flux and dpa responses in this case - playing variance reduction according to parameters produced with the DSA method for fixed source and multiple responses (many responses in the same simulation). The problem is thus decoupled.

An alternative approach – which is tested here - is to obtain the results within a single calculation. While searching for the inherent source - due to the fact that the system is multiplicative – the detector responses are evaluated re-estimating the fundamental mode during the same run – without any decoupling and avoiding a subsequent fixed source calculation as previously described [3,4].

In this work, the new approach is compared to the standard procedure involving decoupling, for a number of neutron and gamma flux and dpa responses.

Neutron and gamma contributions to fast flux and dpa are evaluated at different points on the vessel surface of a Gen-III nuclear power reactor, by means of the MCNP transport code (versions 5-1.4 and 6.1) [5,6].

Results are presented and some characteristic features of the innovative method are shown, emphasizing the enhancements which are of interest for damage calculations as well as for deeper penetration problems concerning radiation shielding and decommissioning.

2. Structure of the Report

This report is divided into two parts.

The first part concerns the ongoing application of DSA Variance Reduction method to a Gen-III nuclear reactor core. Standard (decoupled) and innovative (single eigenvalue calculation) methods are employed and for both of them DSA variance reduction parameters are utilized.

The second part concerns a shielding benchmark calculation, the PCA-Replica experiment, whose purpose is to evaluate neutron cross-section libraries. Fixed source calculations are performed and DSA variance reduction parameters are used. The external source does not require decoupling in this case.

3. Gen-III Nuclear Reactor Analysis

3.1 Reactor Model and Responses

In this work, attention is focused on the evaluation of the damage caused by both neutron and gamma fluxes on the inner surface of the vessel. The model of the Gen-III reactor is prepared by means of the Monte Carlo code MCNP: detailed 3D geometrical description is implemented for the reactor core, the reflector and the inner vessel. The internals are modeled as well as the reactor pit. Reference for model preparation is based on data available to the authors (see acknowledgement).

Composition of the core corresponds to the end-of-cycle configuration, referred to the equilibrium cycle. Definition of fuel materials are assigned to each assembly and gadolinium rods are considered. No axial burn-up effect is taken into account. The geometry of the assemblies is detailed pin-by-pin, as in figure 1. Pressure vessel and reactor core are described in figure 2. Dose responses are requested at the inner vessel surface and at core mid-plane, at four angular positions: 0 degrees, 22.41 degrees, 36.26 degrees, 45 degrees. These locations are chosen in order to determine where the neutron and gamma fluxes reach a maximum value.

The nuclear data set utilized is ENDF/B-VII.1 [7] evaluated at both 293 K and 600 K for cold regions and hot portions inside the core, respectively. S(α,β) Data for thermal neutrons are from ENDF/B-VII.0 [8] for water at both 293 K and 600 K – for reasons of format compatibility between MCNP5 and MCNP6.

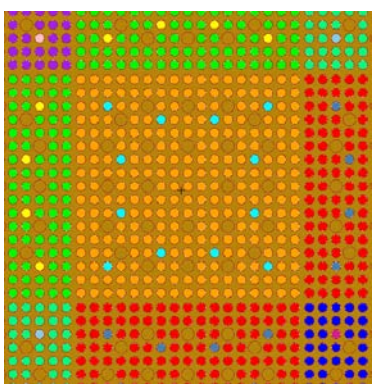

Figure 1.
MCNP model of the pin-by-pin geometry of the assemblies

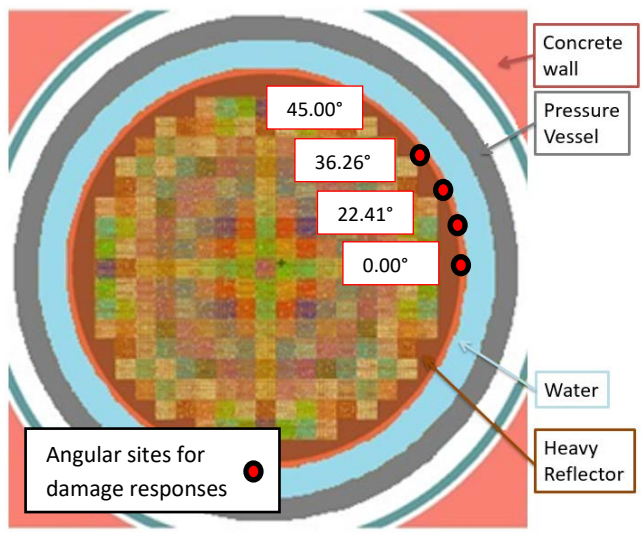

Figure 2.
MCNP reactor model and outside core (at core mid-plane)

The responses of interest are the following:

- neutron dpa with a response function for steel [9,10]
- neutron flux above 1 MeV
- neutron flux above 100 keV
- gamma dpa, with a response function for iron defined over 14 energy groups (threshold 700 keV) [11]

All responses are requested at the four angular positions; thus 16 tallies are considered in total.

3.2 Methodology

Variance reduction games are always required to perform deep penetration problems, and tools have to be employed to produce the variance reduction parameters which provide splitting and Russian roulette at each surface crossing in phase space.

The method utilized here is the Direct Statistical Approach (DSA). Developed for fixed source problems, it has recently been implemented also for multiplicative systems and thus for single calculations in which the fundamental mode flux is regenerated together with particular responses outside the multiplicative zone.

The DSA optimizes splitting and Russian roulette parameters at surfaces in space and in energy, either independent of, or dependent on, the weight of the progenitor arriving at the surface [2]. An important feature of the DSA is the capability of estimating the second-moment, in contrast to classical approaches that rely on the first-moment.

The rationale behind the algorithm and the mathematical method is the optimization in terms of a trade-off between over-splitting and under-splitting. Over-splitting tends to waste time; under-splitting induces too high variance per source history instead.

The DSA allows to deal with many responses, producing variance reduction parameters for a number of objectives simultaneously: this feature is called the multi-response capability. Conceived for fixed source problems, the multi-response capability has been implemented also for fundamental mode simulations.

The method relies on the utilization of both “local” and “global” responses. While in fixed source calculations only local responses are present, both local and global are considered in the case of the single fundamental mode calculation [12], the global responses being required in the fissile zone to maintain the fundamental mode. Conversely, local responses (ex-core) are related to detectors or particular results requested by the user.

Superhistories are employed to extend each cycle by increasing the number of fission generations between normalization points in the source-iteration scheme. (It has been found [13] that employment of superhistories dampens to acceptably low levels fluctuations in the fundamental mode that are stimulated by the variance reduction.)

The damage responses are determined through the following two calculational approaches:

1) Decoupled approach: an analog fundamental mode calculation produces the source that is then employed in a second step in which variance reduction parameters are produced with the DSA (in fixed source mode) and damage responses are generated.

2) Non-decoupled approach: a simulation generates the damage responses in a single calculation (with the DSA in eigenvalue mode). This utilizes variance reduction parameters within a fundamental mode simulation.

3.3 Standard Decoupled Approach

The standard approach for evaluation of ex-core responses consists on a two-step procedure.

First, the inherent source which is related to the critical configuration of a multiplicative system is found. This constitutes the first step and it is carried out in analog form – namely distributions utilized for the sampling process are according to physical laws and no biasing is present.

Fission reaction rates are requested for a particular binning of the fuel domain. The pattern normally used is a pin-by-pin subdivision together with an axial binning of the fuel pins. The source is constructed through tallies over those volumes and converted to a source file by means of an interface code.

Afterwards, a fixed source problem is solved using the previous tally output as a source term. Variance reduction parameters are produced during this second step and optimized for the required responses.

This two-step approach contains some approximations based on certain hypotheses:

- the binned source has a pin-by-pin pattern with a given axial discretization
- the source in each bin is homogenized both radially and azimuthally

- the fixed source has a constant energy distribution

The impact and the limits of this approach constitute the subject of the ongoing work reported here.

3.3.1 Fundamental Mode Calculation

The fission source is produced during a fundamental mode calculation, through 1200 cycles consisting of 10^6 histories each – with no inactive cycles since the transient stage of generating the fundamental mode source was already made. Only neutrons are transported and neutron fission production is tallied on a pin-by-pin pattern in all fuel assemblies in 52 axial bins. The length of the bins is about 3-4 cm at the core bottom and about 10-11 cm from some 150 cm below core mid-plane to 150 cm above core mid-plane. Then, in the upper part of the active zone, the length of the bins is 5-8 cm.

The relative standard deviation provided by MCNP for fission neutron production - without taking into account the correlation between the cycles - is below 5% for about 55% of the bins, 5%-10% for 18% of the bins, and the remaining 18% of the bins show a relative standard deviation of 10%-20%.

3.3.2 Fixed Source Calculation

Following the fundamental mode step, a fixed source simulation is performed in which the only source term considered is constituted by the fission neutrons, previously tallied. (For gamma responses, the activation of structures outside the core is not taken into account in this study, although in principle it is not negligible).

The results of the previous calculation are manipulated through an external Fortran routine, that prepares the customized fixed source, according to the core pin-by-pin pattern. Previous studies showed that a flat radial distribution within an assembly leads to an overestimation of the responses outside the vessel [14]. Thus, in this analysis a pin-by-pin pattern is preferred together with an axial binning to provide each pin with its own axial variation. No radial subdivision is made in each pin. The source position is sampled employing a patch to MCNP that reads the output from the first step while the source energy distribution is taken as the standard Watt spectrum for thermal fission. The damage responses previously described are requested in the second calculation step. Then, appropriate variance reduction parameters are prepared with the DSA (fixed source version) and optimized for all tallies simultaneously with the multi-response capability [2]. These parameters can then be converted to a Weight Window to be implemented in a standard MCNP input.

There are 7 Weight Window energy groups for neutrons and 4 for photons, with upper limits for neutrons: 1 eV, 1 keV, 20 keV, 0.2 MeV, 2 MeV, 5 MeV, 20 MeV and upper limits for photons: 1.5 MeV, 3 MeV, 5 MeV, 20 MeV (with a 700 keV threshold). The fixed source simulation is run up to a total of 10^{10} histories.

3.4 Single Eigenvalue Calculation

So as to avoid decoupling and the approximations inherent in such an approach, a single fundamental mode simulation is performed with the damage responses at the vessel surface and with the variance reduction parameters generated by the DSA.

Employing variance reduction normally distorts the fundamental flux shape. To mitigate this, additional global responses – distinguished from the local vessel damage responses – are inserted inside the core: in our case the core is subdivided into 4 non-equal axial segments and 4 radial segments and thus 16 in-core fission-heating tallies are requested.

There is then a trade-off between a necessary distortion of the particle population aimed at the local responses (damage tallies) and the fundamental mode restoration according to the global in-core responses (fission heating) [3,4,12].

It was found furthermore that the fundamental mode could only be properly balanced through the employment of superhistories [13]. Here a superhistory of 10 fission generations was employed, a number shown to be sufficient to achieve this goal [13].

3.5 Results and Comparison

Monte Carlo results obtained through both the single eigenvalue approach and the decoupled approach are compared. The decoupled approach is considered as reference, since it is common practice in ex-core problems. Notwithstanding, the decoupled approach implies a certain degree of approximation:

Firstly, there is the source discretization: the radial homogenization of the source throughout each pin does not take into account that neutron production is dominant in the outer part of the pin. (Instead we have seen that axial binning tends to be less important for most ex-core responses.)

Secondly the adoption of a single fission spectrum (^{235}U Watt, thermal fission) certainly represents an approximation as there is a non-negligible quantity of Pu in the core.

The DSA method in a single fundamental mode calculation attempts to quantify such approximations.

Note all the reported results have a relative standard deviation less than 1%. (Note that in the decoupled approach, the statistical error on the neutron source is ignored.) Furthermore, the two approaches are statistically independent. Primarily the standard decoupled approach shows a systematic underestimation of the results, compared to the single fundamental mode calculation: this occurs for all tallies at the core mid-plane and for both neutron-based and gamma-based responses.

The neutron flux (above 1 MeV) differs between 10% to 14%, going from the 45° to the 0° position, as shown in figure 3. Considering neutron dpa evaluations the trend is similar (see figure 4). Comparison yields an underestimation of the standard decoupled approach of 11%-12% with respect to the single eigenvalue approach. Conversely, the gamma dpa results are less sensitive to the simulation approach. In fact, the standard decoupled approach underestimates the gamma dpa by only some 2% to 5%, as reported in figure 5.

The systematic underestimation of the standard method – with respect to the DSA – constitutes the main result of the work.

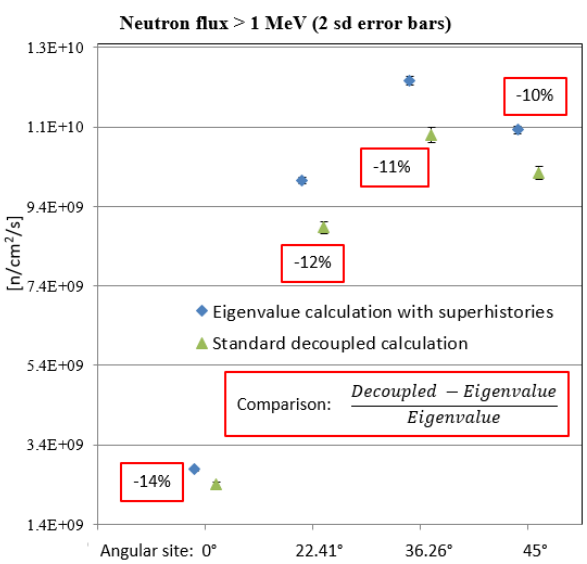

Figure 3.
Single eigenvalue and decoupled approaches:
comparison of neutron flux (above 1 MeV)

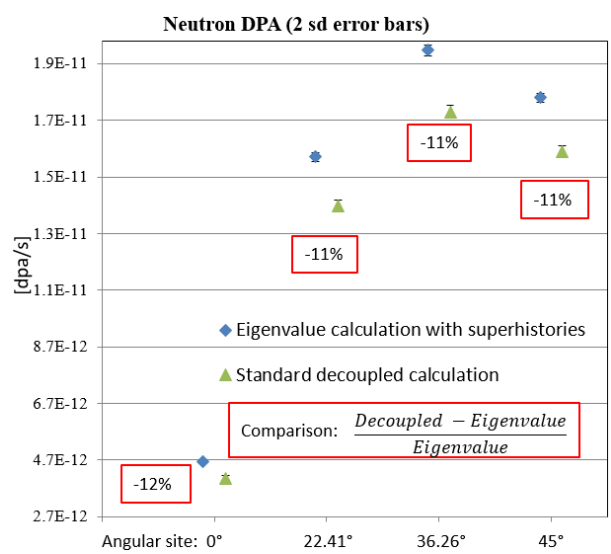

Figure 4.
Single eigenvalue and decoupled approaches:
comparison of neutron dpa

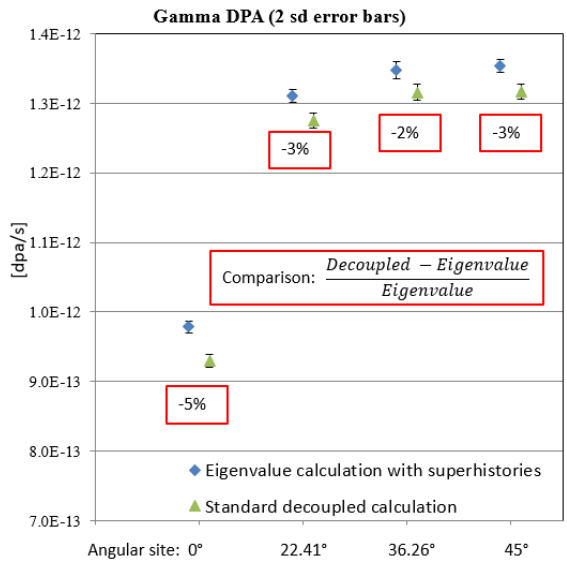

Figure 5.
Single eigenvalue and decoupled approaches:
comparison of gamma dpa

3.6 Conclusions

Within the framework of nuclear safety analyses supporting licensing and design of existing and innovative nuclear reactors, Monte Carlo codes are utilized to obtain detailed responses: in particular, fast neutron flux and dpa dose delivered by both neutrons and gammas to the pressure vessel.

Therefore, innovative methods to improve calculation efficiency as well as precision of the results are key tools to enhance safety analyses.

Currently, a decoupled approach is used to obtain ex-core responses in critical systems, through a first fundamental mode simulation in which a source is prepared for a subsequent decoupled fixed source calculation - provided with ad-hoc variance reduction parameters.

The innovative approach here proposed is based on the Direct Statistical Approach (DSA) [3,4,12,13]. It is implemented as a patch applied to MCNP and allows variance reduction for multiple responses within the same fundamental mode simulation without the need for decoupling.

This approach is applied here to a Gen-III PWR model, in which neutron and gamma damage responses are requested at the vessel surface at different angular positions at the core mid-plane.

Results show the following trend: the decoupled approach underestimates the tallies compared to the single eigenvalue approach by about 10%-14% for neutron-based responses (flux or dpa). Gamma dpa results are underestimated by less than 5%.

In addition, it is worth remarking that the calculation times of the two methods are similar.

Further simulations and tests are necessary in order to establish which approximation in the decoupled approach is mainly responsible for the differences.

This method can then provide an enhanced and more efficient methodology to support safety analyses of nuclear power plants, with interesting possible applications both in the radiation shielding and decommissioning domains.

3.7 Acknowledgments

This work was carried out in the context of a collaboration between ENEA and IRSN (French Institute of Radiological Protection and Nuclear Safety) concerning the evaluation of ex-core responses in Gen-II and Gen-III PWRs. Furthermore IRSN provided the Gen-III PWR MCNP model used in this work.

The computing resources and the related technical support used for this work have been provided by CRESCO/ENEAGRID High Performance Computing infrastructure and its staff*. CRESCO/ENEAGRID High Performance Computing infrastructure is funded by ENEA, the Italian National Agency for New Technologies, Energy and Sustainable Economic Development and by Italian and European research programs, see http://www.cresco.enea.it/english for information.

*G. Ponti et al., Proc. of the 2014 International Conference on High Performance Computing and Simulation, HPCS 2014, 1030

3.8 References

[1] A. Ballesteros et al., “The Role of Pressure Vessel Embrittlement in the Long Term Operation of Nuclear Power Plants”, Nuclear Engineering and Design, 234 (2012) 63-68

[2] K.W. Burn, “Optimizing Monte Carlo to multiple responses: The Direct Statistical Approach, 10 years on.”, Nucl. Technol. 175, (2011) 138–145.

[3] K.W. Burn, “Optimizing variance reduction in Monte Carlo eigenvalue calculations that employ the source iteration approach”, Annals of Nuclear Energy, 73 (2014) 218-240

[4] K.W. Burn, “A correction and a clarification to ‘Optimizing variance reduction in Monte Carlo eigenvalue calculations that employ the source iteration approach’”, Ann. Nucl. Energy, 85, 776 (2015)

[5] X-5 Monte Carlo Team, “MCNP – A General Monte Carlo N-Particle Transport Code”, Version 5, LA-UR-03-1987 (2008)

[6] T. Goorley et al., “Initial MCNP6 Release Overview – MCNP6 version 1.0”, LA-UR-13-22934, (2013)

[7] M.B. Chadwick et al., “ENDF/B-VII.1 Nuclear Data for Science and Technology: Cross Sections, Covariances, Fission Product Yields and Decay Data”, Nuclear Data Sheets, 112 (2011), 2887-2996

[8] M.B. Chadwick et al., “ENDF/B-VII.0: Next Generation Evaluated Nuclear Data Library for Nuclear Science and Technology”, Nuclear Data Sheets, 107 (2006), 2931-3060

[9] Yu. A Korovin et al., "BISERM-2. Nuclear Data Library for Evaluation of Radiation Effects in Materials Induced by Neutrons of Intermediate Energies", IAEA-NDS-203 (March 1997)

[10] A. Konobeyev, K. Voukelatou, "Displacement Cross-Sections for Materials Irradiated with Neutrons and Protons at the Energies up to 1 GeV". Private communication, April 2003

[11] E.D. Blakeman, "Neutron and Gamma Fluxes and dpa Rates for HFIR Vessel Beltline Region (Present and Upgrade Designs)", ORNL/TM-13693 (Nov. 2000)

[12] K.W. Burn, “Estimating Local In- and Ex-Core Responses within Monte Carlo Source Iteration Eigenvalue Calculations”, PHYSOR 2014, JAERI-Conf 2014-003 (2014)

[13] K.W. Burn, P. Console Camprini, “Radiation transport out from the reactor core: to decouple or not to decouple”, ICRS-13 & RPSD-2016, Paris, November 2016

[14] M. Brovchenko et al., “Neutron-gamma flux and dose calculations for feasibility study of instrumentation implementation in the European Pressurized Reactor (EPR)”, ICRS-13 & RPSD-2016, Paris, November 2016

4. PCA-Replica Shielding Benchmark

4.1 Introduction

Within the framework of nuclear engineering design and safety evaluations, an important role is performed by shielding calculations. These analyses are utilized to support both the exploitation of existing plants (in particular their lifetime extension as well as decommissioning strategies) and the design of innovative nuclear systems.

Thermal and mechanical properties of relevant structural materials are modified by irradiation conditions and fluence, mainly degrading component performances and endurance. In fact, structural materials inside a nuclear power reactor experience both radiation hardening and shift of ductile-brittle transition temperature (DBTT) which tends to increase as we move towards operating conditions. Designers consider that potential damage depends mainly on the magnitude of the neutron fluence (and especially on the portion above 100 keV) received by an exposed component.

In particular, the pressure vessel is a crucial component which must not fail. It therefore determines the nuclear plant lifespan. Moreover, internals are subjected to high irradiation doses as well, and if they are not replaceable, deserve particular analysis and controls during the operating life of the plant [1].

For these reasons, radiation-resistant materials are selected for key components. Numerical analysis is normally carried out right from the early design phase to evaluate radiation damage, from microscopic phenomena up to macroscopic analysis at the component scale [2]. Results are then compared with data from irradiation experiments and material tests.

The main input for numerical damage estimation to mechanical components is dose evaluation and the determination of the neutron and gamma irradiation field is the key part of the analysis. The preferred approach relies on transport codes and in particular Monte Carlo methods, that can treat nuclear data in a continuous fashion and accept three-dimensional complex geometries.

In order for the numerical tools to provide neutron flux and dose evaluations with a properly estimated uncertainty - mainly related to input data - benchmark calculations are usually prepared and updated for each issued nuclear data set [3]. Experiments are designed to reproduce simple and representative geometry and materials so as to be able to extrapolate the results to full-size components of the nuclear facility: nuclear power plants, research reactors, radioactive sources, waste storage repositories.

In addition to vessel degradation issues, nuclear reactors require evaluations of the radiation penetration outside the pressure vessel, to provide designers with specific information concerning doses to personnel during operation but also to electronic equipment and diagnostic and control devices. Therefore, both in-core and ex-core responses require validation benchmarks to support the calculations.

Experimental shielding mock-ups for benchmark purposes involve materials of interest (structural, coolant, moderator…) based on the technology of interest [4,5]. Thus, measurements in benchmarks have to be carried out with a high degree of accuracy in order to provide sufficiently accurate results to highlight numerical performances, through comparison between calculation and measurement [6].

The present work concerns an analysis of iron and water as structural and moderator materials in GenII and GenIII LWR's. This shielding experimental benchmark is provided by the Nuclear Energy Agency (NEA) and assembled in the Shielding Integral Benchmark Archive and Database (SINBAD) [7]. In particular, the present study deals with the PCA-Replica experimental benchmark [8] and the simulations were carried out with the MCNP6.1 Monte Carlo transport code [9]. Variance reduction techniques were employed and variance reduction coefficients in the form of weight window parameters [10] were produced by means of the DSA method [11].

Simulation responses to be compared with experimental results are: dosimeter readings (10 positions) and neutron spectra (2 positions).

The nuclear data utilized in this calculation are subdivided into the two categories: nuclear data sets for neutron transport and dosimetry data for neutron response functions. The results presented compare the following nuclear transport libraries: ENDF/B-VI.6 [12], ENDF/B-VII.1 [13], JEFF-3.1 [14], JEFF-3.1.2 [15], JEFF-3.2 [16] and JENDL-4.0 [17]. For each of these transport libraries, dosimetry data tables for dosimeter readings – namely reaction rates – have been generated with the following files: 531DOS, 532DOS, LLLDOS [18], IRDF2002 [19] and IRDFFv1.05 [20].

4.2 PCA-Replica Benchmark

The PCA-Replica shielding benchmark is part of the Shielding Integral Benchmark Archive and Database (SINBAD) at the Nuclear Energy Agency (NEA-1517/93) [7]. The PCA-Replica experimental campaign has been carried out at the NESTOR research reactor at UKAEA Winfrith in the early 1980's [8]. The experiment was prepared in the ASPIS irradiation facility – inside NESTOR – in which a movable trolley carried the experimental device (fission plate and shielding mock-up) (Fig. 1).

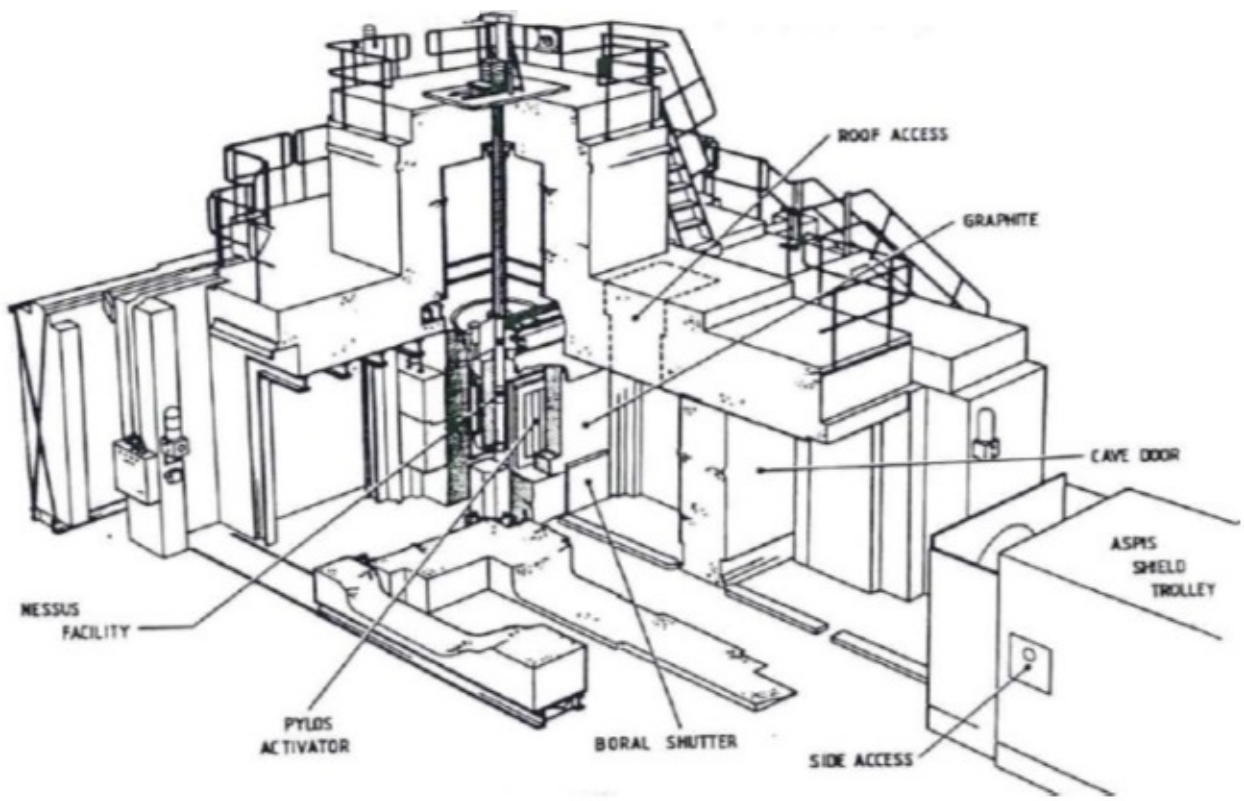

Figure 1. NESTOR reactor and the ASPIS shield trolley [8]

PCA-Replica is an iron/water shielding benchmark since the objective is to evaluate the uncertainty in numerical simulations of the neutron flux inside the thermal shield and pressure vessel – which are mainly composed of iron - in light water reactors. Through evaluation of the neutron flux it is possible to determine dose, nuclear heating and atomic displacement in materials. In addition, the

characterization of the neutron irradiation field in the ex-core region – namely in the void zone between pressure vessel and biological shield – is an objective of the evaluation.

The experimental geometry consists of a simple multilayer domain composed of the materials of interest: mild steel, stainless steel, light water and a void region. Materials are listed according to neutron penetration away from the source as follows:

- planar neutron source (fission plate)
- water gap (12 cm)
- thermal shield sample (6 cm)
- water gap (13 cm)
- pressure vessel sample (22 cm)
- void box
- water pool

The experimental mock-up is immersed in water and placed on the ASPIS movable trolley (Fig. 2) [8].

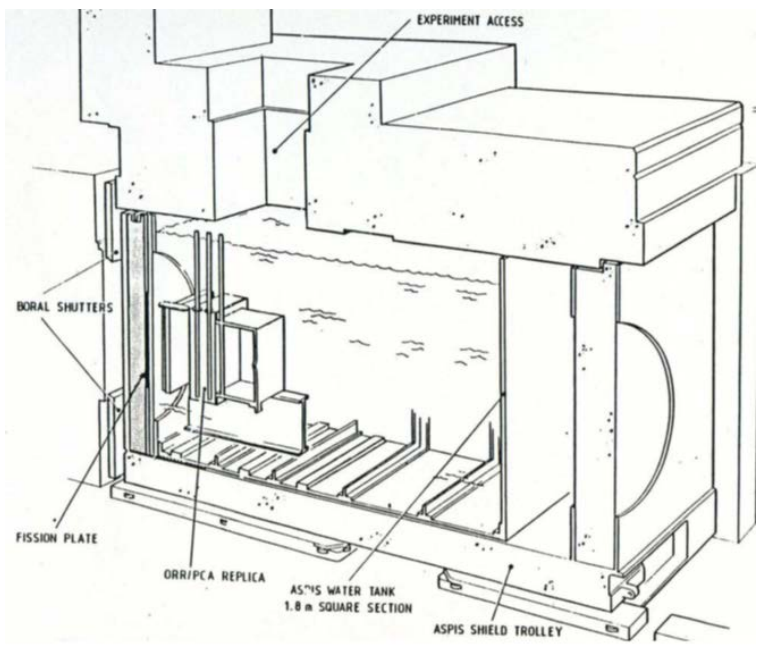

Figure 2. PCA-Replica mock-up installed inside the ASPIS facility [8]

The fission plate was designed in order to employ a precise source characterization through a fission spectrum. In fact, PCA-Replica was intended to provide support and verification to the previously performed PCA experiment carried out at ORNL in 1978 [21]. This was sponsored by the US NRC within the framework of the Surveillance Dosimetry Improvement Program (SDIP). An experimental campaign was carried out to validate nuclear data and methodology for dose estimation to the reactor pressure vessel (RPV), thermal shield (TS) and ex-core neutron leakage for ex-core irradiation issues. Despite a simple experimental mock-up, a more precise source specification was preferred for benchmark requirements.

Therefore, the Winfrith research group decided to prepare a new experimental configuration, in which a fission plate situated outside the NESTOR core could be irradiated by the thermal neutron leakage flux. This provided a well-defined source with a fission spectrum.

4.3 Geometry of the System

The PCA-Replica geometry is basically a multi-layer installation of steel specimens representing a thermal shield and pressure vessel immersed in light water. The problem consists of a series of slabs made of steel placed parallel to the x-y plane (where y is the vertical direction), while the main direction of the problem is along the z axis (the horizontal cross section is shown in Fig. 3).

The NESTOR core is not represented but is situated above the upper part of Fig. 3. The neutron flux diffuses from the core through the shutter made of graphite (zone 1) and the aluminum window (zone 2). Zone 19, concrete, represents part of the NESTOR shield. The void region – zone 3 – indicates the space between the fixed portion (at the top of the picture) and the movable trolley (all parts below zone 20).

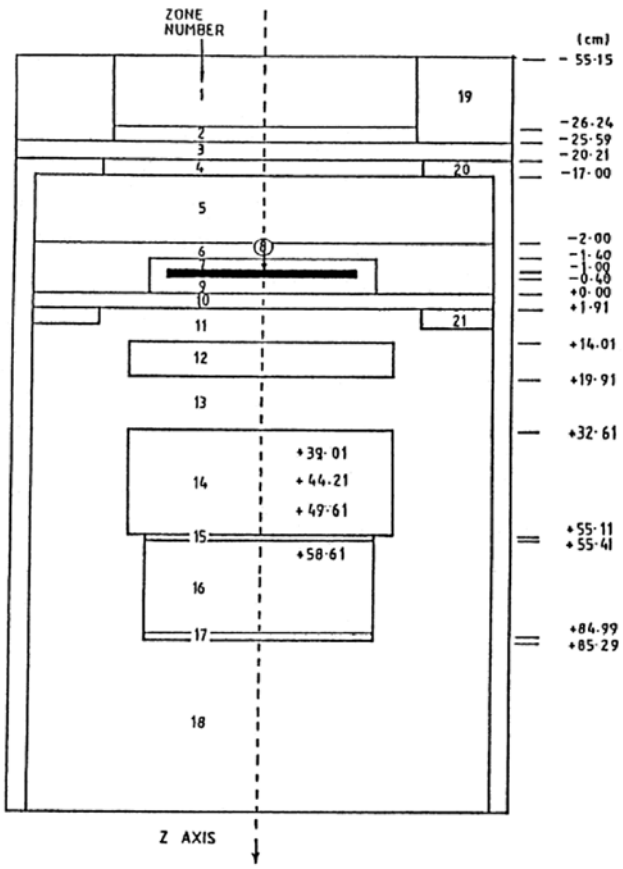

Figure 3. PCA-Replica geometry cross-section (horizontal cross section x-z) [22]

The x-y dimensions of the zones shown in Fig. 3 are provided in Table 1. All zones are parallelepipeds apart from zone 4 which is circular.

Zone 20 represents the trolley sides; they are made of mild steel and contain all the test facility. Neutrons from NESTOR core pass through the circular window made of aluminum, zone 4. Then, a graphite layer, zone 5, provides further moderation [23].

The fission plate (zone 8) is inserted in an aluminum cladding about 0.4 cm thick (zones 7 and 9).

Zone 10 is an aluminum barrier, beyond which the water volume is contained. Zone 11 indicates the water layer, 12 cm thick, inside the structure, zone 21 (mild steel). Zone 13, 13 cm thick, is water. (The water layer thickness is a key parameter in a shielding benchmark for water reactor technology. For this reason, the PCA-Replica is referred to as a 12/13 iron/water benchmark.) The metallurgical specimen (zone 12) is made of stainless steel and represents the thermal shield. By contrast, a mild steel sample (zone 14) simulates the reactor pressure vessel [24].

Beyond the pressure vessel sample, zone 16 is void. The thin slabs (zones 15 and 17) are water-tight aluminum layers. Water is in zone 18 and surrounds the specimens. In the real experimental facility, concrete structure is present outside zone 20. Instead in this model, zero albedo is assumed outside zone 20.

Zone	Material	Section	Dimensions [cm]
1	Carbon	Square	119.0 - Side
2	Aluminum	Square	119.0 – Side
3	Void	Square	185.0 – Side
4	Aluminum	Circular	56.06 – Radius
5	Carbon	Square	180.0 – Side
6	Void	Square	180.0 – Side
7	Aluminum	Rectangular	68.5 x 47.5
8	Fuel	Rectangular	63.5 x 40.2
9	Aluminum	Rectangular	68.5 x 47.5
10	Aluminum	Square	180.0 – Side
11	Water	Square	180.0 – Side
12	Stainless Steel	Square	68.5 – Side
13	Water	Square	180.0 – Side
14	Mild Steel	Square	68.5 – Side
15	Aluminum	Square	60.0 – Side
16	Void	Square	59.4 – Side
17	Aluminum	Square	60.0 – Side
18	Water	Square	180.0 – Side

Table 1. Materials and dimensions in x-y plane [8]

In order to better describe the fissile region, zone 8 is further subdivided. The fission plate is actually composed of 52 fuel strips, each 1.016 mm thick and 30.48 mm wide and with a height of 635 mm. They are grouped in clusters of 4 strips each, as shown in the sketch in Fig. 4. The clusters of strips are positioned with a pitch of 30.92 mm. The total thickness of the fission plate in zone 8, including metallic uranium strips and voids, is 6 mm. A cross-section of zones 7, 8 and 9 with a detailed view of fission plates is reproduced at the bottom of Fig. 4.

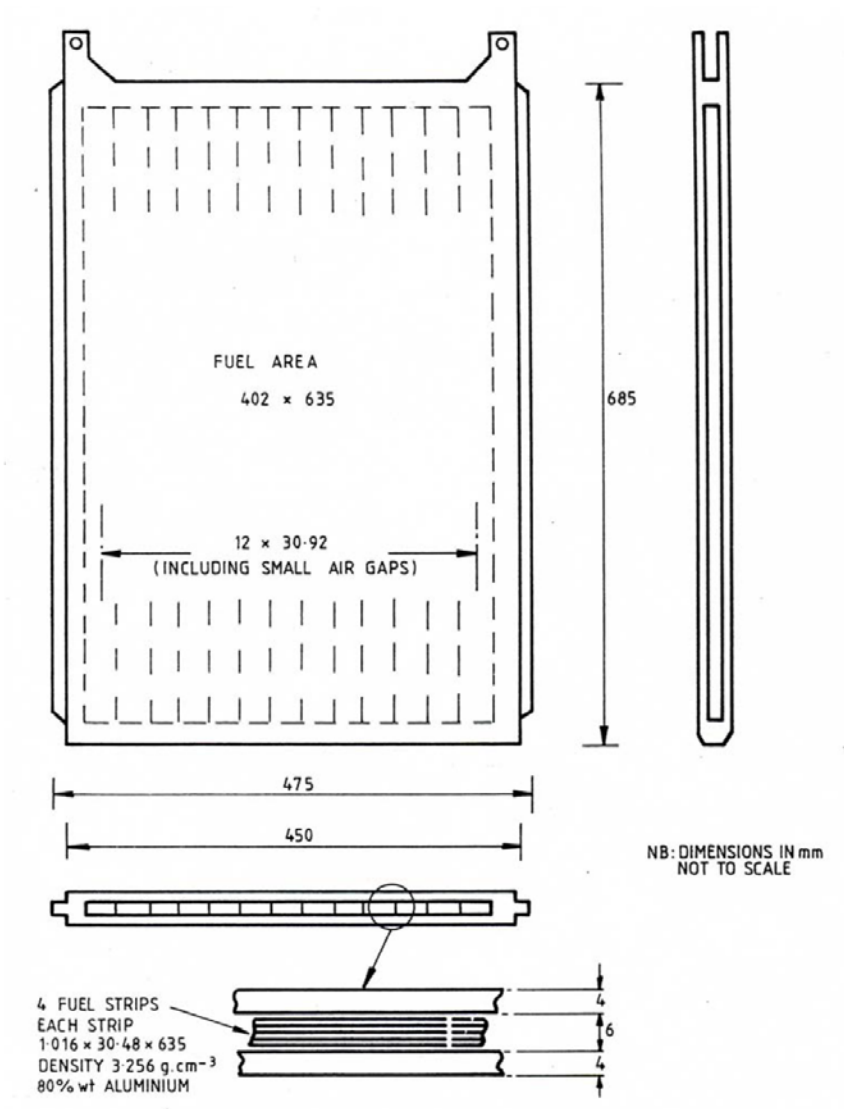

Figure 4. Fission plate geometry: detailed description [8]

4.4 Composition of Materials

The materials utilized in the present benchmark are mainly water and steel. Structural materials, neutron windows (i.e. aluminum) and moderator are then necessary to completely define the calculational mock-up. They are all at room temperature, thus 300 K cross-section nuclear data tables are used. The fission plate is made of 93% enriched uranium in ^{235}U. The isotopic composition of all other elements is natural [25]. The material compositions are shown in Table 2.

Material	Material Density [g/cm3]	Element	Weight [%]	Atomic Density [atoms/cm3]
Graphite	1.65	C	100.0	8.276E+22
Aluminum Cladding	2.70	Al	100.0	6.029E+22
Alloy Fuel*	3.257	Al	80.0	5.818E+22
		U-235	18.6	1.552E+21
		U-238	1.4	1.154E+20
Water	1.0	H	11.19	6.688E+22
		O	88.81	3.344E+22
Stainless Steel	7.88	C	0.017	6.721E+19
		Si	0.44	7.438E+20
		Mn	1.57	1.356E+21
		P	0.025	3.832E+19
		S	0.006	8.884E+18
		Cr	18.4	1.688E+22
		Ni	9.4	7.601E+21
		Mo	0.37	1.831E+20
		Ti	0.009	8.920E+18
		Nb	0.014	7.154E+18
		Cu	0.24	1.793E+20
		Fe	69.509	5.909E+22
Mild Steel	7.835	C	0.22	8.646E+20
		Mn	1.09	9.366E+20
		P	0.01	1.524E+19
		S	0.032	4.711E+19
		Fe	98.648	8.338E+22
Concrete	2.3	Si	33.7	4.120E+22
		Fe	1.4	8.609E+20
		H	1.0	3.407E+22
		O	52.9	1.135E+23
		Al	3.4	4.327E+21
		Ca	4.4	3.770E+21
		Na	1.6	2.390E+21
		K	1.6	1.405E+21

* Uranium enriched to 93 w% in U-235

Table 2. Detailed composition of materials used in the problem [8]

4.5 Neutron Source

The PCA-Replica experiment is driven by a fission plate coupled to the NESTOR core via a thermal column. This source is particularly interesting for the degree of accuracy since the energy distribution is exactly a fission spectrum induced by thermal neutrons.

The shape factor in the x-y plane is defined in Table 3. As we can see it is consistent with the dimensions of zone 8. The source intensity in Table 3 is given in terms of neutrons/cm^3/Watt (Watt refers to the fission plate power) and the relative source intensity is obtained after multiplying the data in Table 3 by the respective volumes. The thickness of the plate is constant over the whole area.

X-axis [cm] / Y-axis [cm]	-20.10 ÷ -12.10	-12.10 ÷ -4.10	-4.10 ÷ 4.10	4.10 ÷ 12.10	12.10 ÷ 20.10
-31.75 ÷ -26.32	4.424E+07	4.418E+07	4.495E+07	4.448E+07	4.560E+07
-26.32 ÷ -20.58	4.609E+07	4.518E+07	4.557E+07	4.535E+07	4.772E+07
-20.58 ÷ -15.44	4.885E+07	4.696E+07	4.744E+07	4.747E+07	5.040E+07
-15.44 ÷ -10.00	5.157E+07	4.885E+07	4.690E+07	4.989E+07	5.293E+07
-10.00 ÷ -3.33	5.393E+07	5.055E+07	5.160E+07	5.217E+07	5.505E+07
-3.33 ÷ 3.33	5.500E+07	5.135E+07	5.252E+07	5.332E+07	5.601E+07
3.33 ÷ 10.00	5.426E+07	5.078E+07	5.179E+07	5.264E+07	5.531E+07
10.00 ÷ 15.44	5.231E+07	4.927E+07	4.996E+07	5.069E+07	5.351E+07
15.44 ÷ 20.58	5.006E+07	4.764E+07	4.806E+07	4.855E+07	5.144E+07
20.58 ÷ 26.32	4.802E+07	4.642E+07	4.684E+07	4.699E+07	4.964E+07
26.32 ÷ 31.75	4.723E+07	4.670E+07	4.778E+07	4.756E+07	4.874E+07

Table 3. Neutron source shape in x-y plane for the fission plate [8]

Considering the source shape in the z direction, region 8 is divided into four parts and the dependence of the source on z is reported in Table 4 as a histogram distribution.

Step	Interval z axis	Value	Error
Spike 1	- 1.00 – - 0.85 cm	1.109	± 0.008
Spike 2	- 0.85 – - 0.70 cm	0.997	± 0.027
Spike 3	- 0.70 – - 0.55 cm	0.939	± 0.020
Spike 4	- 0.55 – - 0.40 cm	0.955	± 0.013
Mean spike	- 1.00 – - 0.40 cm	1.000	± 0.006

Table 4. Neutron source shape in z direction for the fission plate [8]

The geometric characterization of the neutron source is then easily reproduced by implementing in MCNP the discrete shape functions in Tables 3 and 4. Concerning the energy spectrum, a standard Watt fission spectrum with recommended parameters for thermal fission in ^{235}U [9] was employed.

The fission neutron production in the plate is considered proportional to the NESTOR core power – from 1 W to 30 kW – with a good degree of accuracy of about 0.4% over the full power range. The PCA-Replica experiment has been carried out with the NESTOR core at full power – namely 30 kW [8]. The final normalization of the fission plate neutron source is 5.1274480×10^{7} n/sec/NESTOR Watt [8] (2.104×10^{7} fissions/sec/NESTOR Watt multiplied by a mean value of 2.437 n/fission [8]). Note that a total error of 3.8% was assigned to the fission plate output [8].

4.6 Experimental Results

The experimental results produced during the PCA-Replica campaign consisted of the dosimeter readings and the neutron spectra. Since this benchmark is oriented to pressure vessel protection and damage evaluation, particular attention has been paid to the high-energy tail of the neutron spectrum. To this purpose inelastic scattering and proton-recoil dosimeters have been employed with different threshold energies. The response functions utilized are the following:

- ^{103}Rh dosimeters (^{103}Rh(n,n′)^{103m}Rh reaction) with energy threshold around 0.04 MeV;
- ^{115}In dosimeters (^{115}In(n,n′)^{115m}In reaction) with energy threshold around 0.35 MeV;
- ^{32}S dosimeters (^{32}S(n,p)^{32}P reaction) with energy threshold around 1.00 MeV.

The dosimeters were placed at ten positions inside both the water gaps, the cavities within the pressure vessel sample at ¼ and ¾ of its thickness (referred to as T/4 and 3T/4) and the void box after the pressure vessel sample. Their positions are reported in Table 5.

	Reference Location	**Distance from Fission Plate [cm]**	**Reaction Rate/NESTOR Watt [dps/atom]**		
			$^{103}Rh(n,n')^{103m}Rh$	$^{115}In(n,n')^{115m}In$	$^{32}S(n,p)^{32}P$
			Systematic ± 3%	Systematic ± 2%	Systematic ± 4%
1	12 cm Water Gap	1.91	1.69 E -20 ± 3%	-	-
2		7.41	3.78 E -21 ± 3%	-	-
3		12.41	1.40 E -12 ± 3%	-	-
4		14.01	1.27 E -21 ± 3%	-	-
5	13 cm Water Gap	19.91	4.23 E -22 ± 3%	-	-
6		25.41	1.15 E -22 ± 4%	-	-
7		30.41	4.73 E -23 ± 4%	-	-
8	T/4	39.01	2.07 E -23 ± 1%	3.93 E -24 ± 0.9%	1.08 E -24 ± 1.5%
9	3T/4	49.61	5.53 E -24 ± 1.9%	8.23 E -25 ± 1.4%	1.46 E -25 ± 1.9%
10	Void Box	58.61	1.80 E -24 ± 1.6%	2.31 E -25 ± 1.5%	3.73 E -26 ± 1.3%

Table 5. Threshold reaction rates as measured on the horizontal axis (z axis) [8]

Dosimeter readings are provided with a twofold uncertainty: both systematic and stochastic errors are indicated in Table 5 (stochastic are interpreted as 1 standard deviation of a Gaussian distribution).

As far as the neutron source is concerned, the PCA-Replica source comes mainly from the fission plate. However, some background from the NESTOR core is present, although at a low intensity. It is taken into account as follows:

- dosimeter responses in water gaps (positions 1 to 7): 2% more than fission plate alone;
- dosimeter responses in vessel and void (positions 8 to 10): 4% more than fission plate alone.

The neutron spectra have been generated at two positions: inside the vessel sample and in the void box (at the same positions as dosimeters 8 and 10 in Table 5). Spectrum measurements have been made with hydrogen-filled proportional counters together with Ne213 organic liquid scintillators to extend the energy range of spectral measurements above that achievable by gas counters. The experimental results are reported in Table 6. The estimated uncertainty on the unfolded fluxes is not reported in [8]. Thus only the neutron background is considered as a source of uncertainty – as reported above about 4% of the fission plate intensity for these two positions.

Energy Group		**Flux per unit Lethargy/NESTOR Watt**	
Lower limit [MeV]	**Upper limit [MeV]**	**T/4 position**	**Void Box position**
0.052	0.059	6.8	0.45
0.059	0.067	6.0	0.68

0.067	0.076	6.7	1.21
0.076	0.086	6.7	1.15
0.086	0.097	6.3	0.58
0.097	0.111	7.4	0.87
0.111	0.126	9.0	1.48
0.126	0.143	10.0	2.22
0.143	0.162	9.0	1.62
0.162	0.183	10.0	1.92
0.183	0.207	9.2	1.60
0.207	0.235	10.3	1.49
0.235	0.266	11.7	2.22
0.266	0.302	14.0	3.13
0.302	0.342	17.0	3.31
0.342	0.388	16.0	2.99
0.388	0.439	13.7	1.88
0.439	0.498	16.2	2.33
0.498	0.564	19.0	2.74
0.564	0.639	23.9	4.12
0.639	0.724	20.3	3.19
0.724	0.821	17.1	1.75
0.821	0.930	15.7	1.93
0.930	1.054	15.5	1.69
1.054	1.194	15.3	1.53
1.194	1.353	13.7	1.16
1.353	1.534	13.8	0.94
1.534	1.748	13.3	0.78
1.748	1.969	11.9	0.61
1.969	2.231	11.7	0.46
2.231	2.528	11.2	0.35
2.528	2.865	9.2	0.27
2.865	3.246	6.9	0.18
3.246	3.679	4.4	0.13
3.679	4.169	4.8	0.10
4.169	4.724	5.0	0.09
4.724	5.353	4.2	0.09
5.353	6.065	3.5	0.07
6.065	6.873	2.2	0.06
6.873	7.788	1.5	0.03
7.788	8.825	1.1	0.02
8.825	10.0	0.2	0.01

Table 6. Neutron spectra as measured at T/4 and Void Box positions [8]

4.7 Calculational Methodology

The PCA-Replica benchmark has been simulated with the Monte Carlo code MCNP6.1 [9] which allows a reasonably faithful representation of the geometry of the facility.

A Cartesian fission source in x-y-z coordinates has been implemented and subsequent fissions in the fission plate are treated as absorptions. Neutron-only calculations have been run.

Simulations were run with 10^9 histories each with a computation time of about 200 min-CPU on a HPC supercomputer CRESCO4 at ENEA Portici Research Center [26].

Variance reduction techniques were implemented. Firstly, an energy cutoff was enabled with a threshold of about 50 keV which takes into account both the energy threshold of the detectors and the lowest energy group in the spectrum counters. Then the multi-response capability of the DSA (Direct Statistical Approach) [11] was employed to produce variance reduction parameters in the form of a weight window [10]. As far as the detector responses were concerned, the calculational (i.e. Monte Carlo statistical) uncertainty was then below 1% even for the ^{32}S detector position in the void box – which is the farthest position from the fission plate and has the highest threshold energy. (We remind ourselves that the uncertainty in the source intensity (§5) is 3.8%.)

4.8 Nuclear Data Sets

The present benchmark has been utilized to test the following types of nuclear data:
- neutron interaction tables for the particle transport;
- dosimetry interaction tables for the dosimeter readings.

All the data are at room temperature – namely 300 K. For each neutron interaction library, every dosimetry table was tested. The following neutron interaction and dosimetry libraries have been employed:

Neutron interaction tables:
- ENDF/B-VI.6 [12]
- ENDF/B-VII.1 [13]
- JEFF-3.1 [14]
- JEFF-3.1.2 [15]
- JEFF-3.2 [16]
- JENDL-4.0 [17]

Dosimetry interaction tables:
- 531DOS [18]
- 532DOS [18]
- LLLDOS [18]
- IRDF2002 [19]
- IRDFF-v1.05 [20]

The dosimetry tables 531DOS and 532DOS are based on ENDF/B-V. LLLDOS is based on ACTL from LLNL. 531DOS and 532DOS do not include ^{103}Rh(n,n')^{103m}Rh, while LLLDOS does not include ^{115}In(n,n')^{115m}In. In contrast, the ^{32}S(n,p)^{32}P reaction is present in all three dosimetry sets. IRDF2002 and IRDFF-v1.05 are more recent IAEA evaluations, although originally based on ENDF/B-V, which include all dosimetry cross-sections used in this benchmark.

It should be mentioned that the ^{115}In(n,n')^{115m}In cross-sections in 531DOS and 532DOS are identical, thus only one is reported in the results. Also the ^{32}S(n,p)^{32}P cross-sections in 532DOS and LLLDOS are identical below 14 MeV and therefore only 532DOS is reported. ^{103}Rh(n,n')^{103m}Rh and ^{115}In(n,n')^{115m}In differ between IRDF2002 and IRDFF-v1.05 in the value of the energy threshold. Although for ^{115}In(n,n')^{115m}In there is only a very slight difference, they were kept separate in the comparison. Thus the following dosimetry cross-sections were tested:

	^{32}S(n,p)^{32}P	^{103}Rh(n,n')^{103m}Rh	^{115}In(n,n')^{115m}In
531DOS	×		
532 DOS	×		×

LLLDOS		×	
IRDF2002	×	×	×
IRDFF-v1.05	×	×	×

4.9 Comparison between Calculation and Measurement

The results for the Dosimeter responses are shown in the following D series of fifteen Figures. The dosimeter reaction rates have been evaluated along the central axis, even at positions where the real dosimeters are not placed during the experiment. This illustrates the reaction rate trend through the water and the steel samples.

Figs. D.E7.1, D.E7.2, D.E7.3, D.E7.4 and D.E7.5 show the comparison between calculation and measurement with ENDF/B-VII.1 transport neutron cross-sections for the five dosimetry files: 531DOS, 532DOS, LLLDOS, IRDF2002 and IRDFF-v1.05 respectively. Figs. D.JF32.1 – D. JF32.5 show the same comparison with JEFF-3.2 transport neutron cross-sections and Figs. D.JL4.1 – D.JL4.5 with JENDL-4.0 cross-sections.

In these fifteen D series Figures, the calculational results are normalized to the NESTOR power, as are the measurements, i.e. the calculational results and measurements are completely independent of each other. Furthermore, the previously cited measurement errors and the stochastic calculational uncertainties are reported in these Figures as 1 standard deviation error bars. However, they are largely invisible. In any case it is apparent from these Figures that there is a good agreement between calculation and measurement. However, because of the scale we are not able to glean any further information.

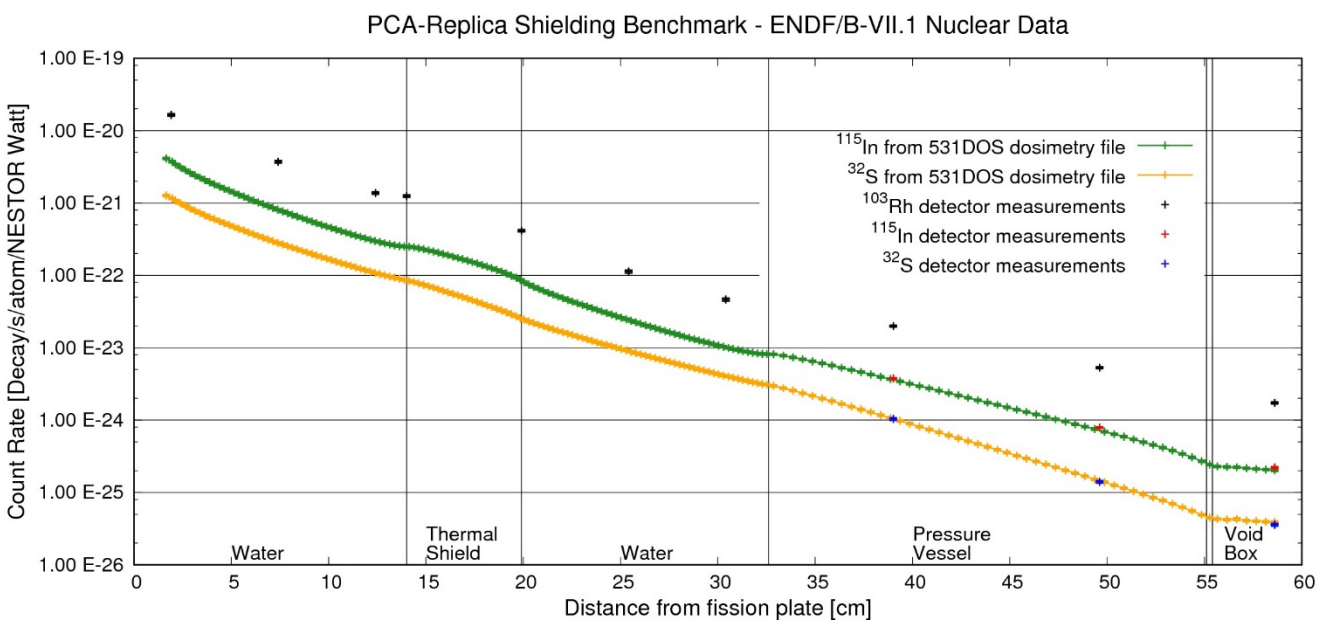

Figure D.E7.1. Dosimeter reaction-rate ENDF/B-VII.1 with 531DOS

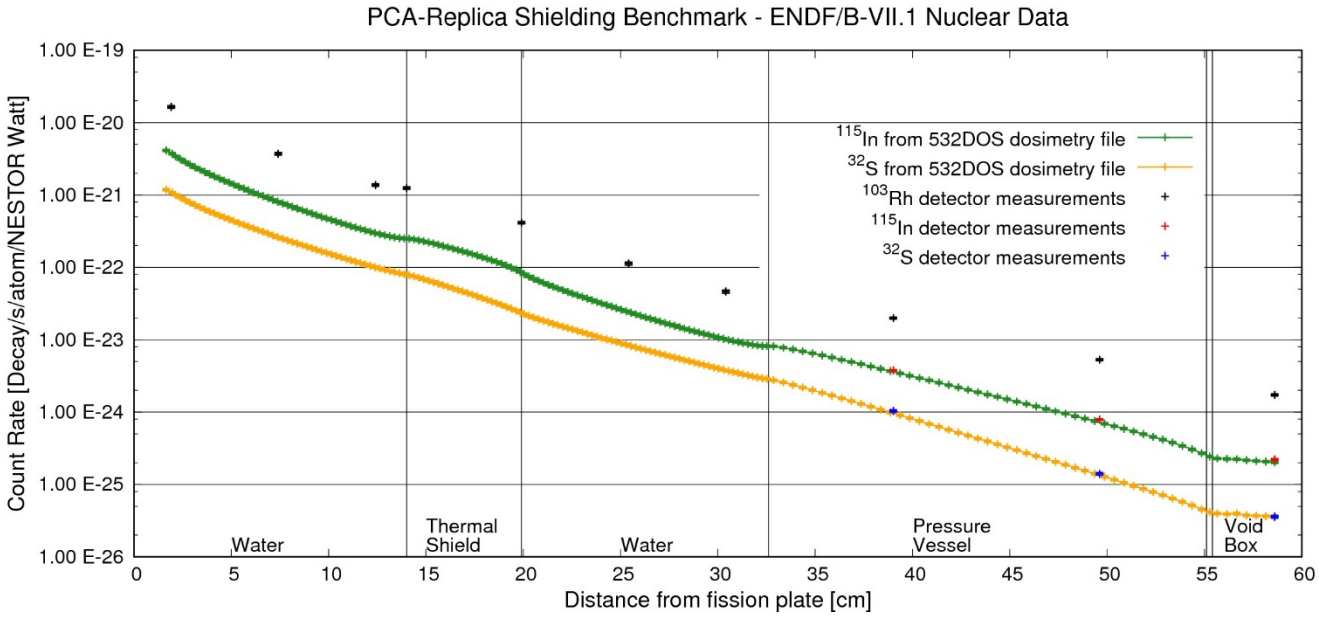

Figure D.E7.2. Dosimeter reaction-rate ENDF/B-VII.1 with 532DOS

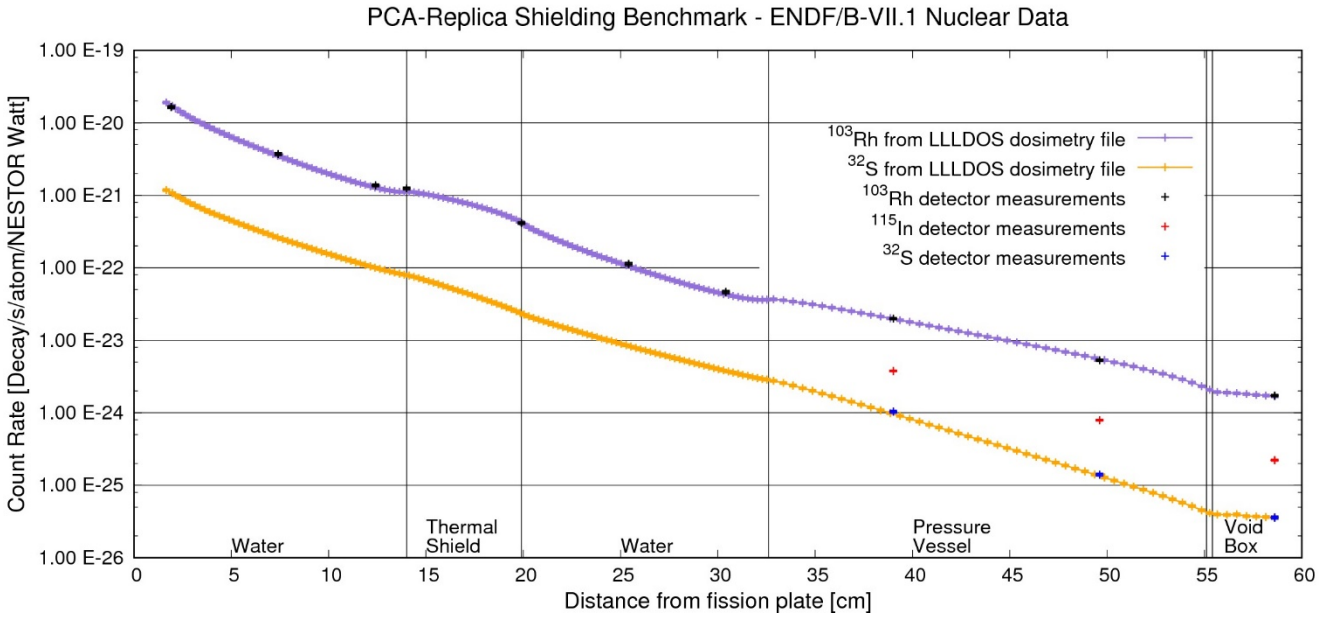

Figure D.E7.3. Dosimeter reaction-rate ENDF/B-VII.1 with LLLDOS

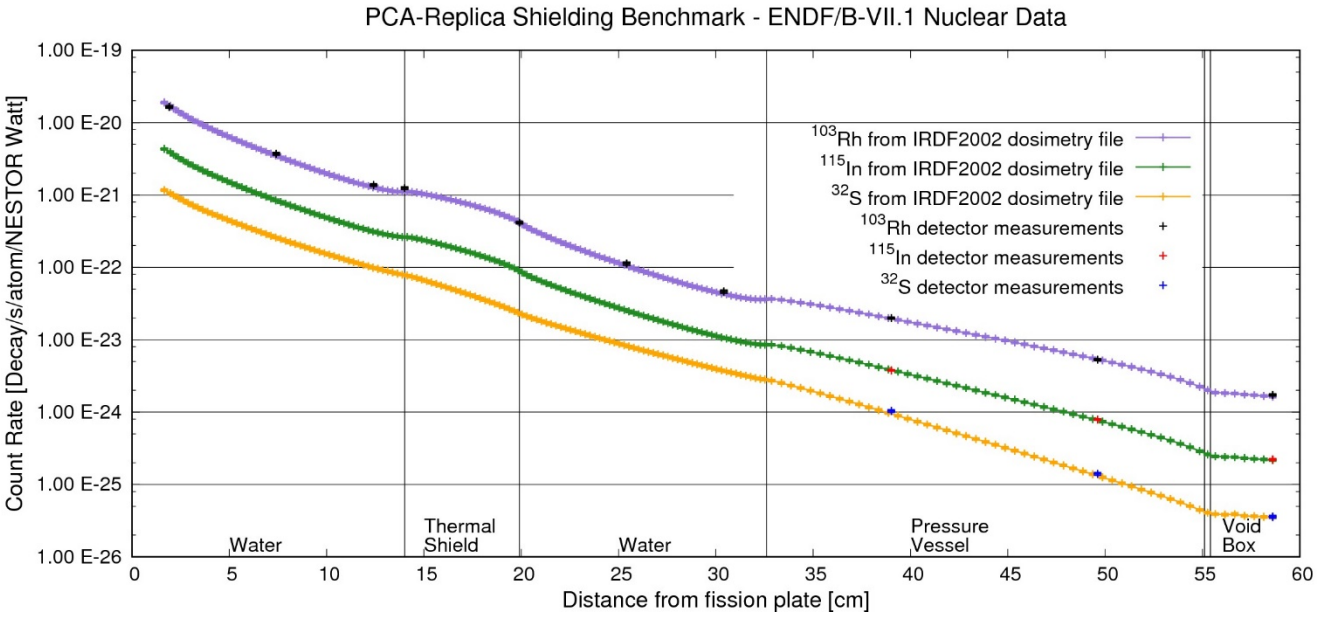

Figure D.E7.4. Dosimeter reaction-rate ENDF/B-VII.1 with IRDF2002

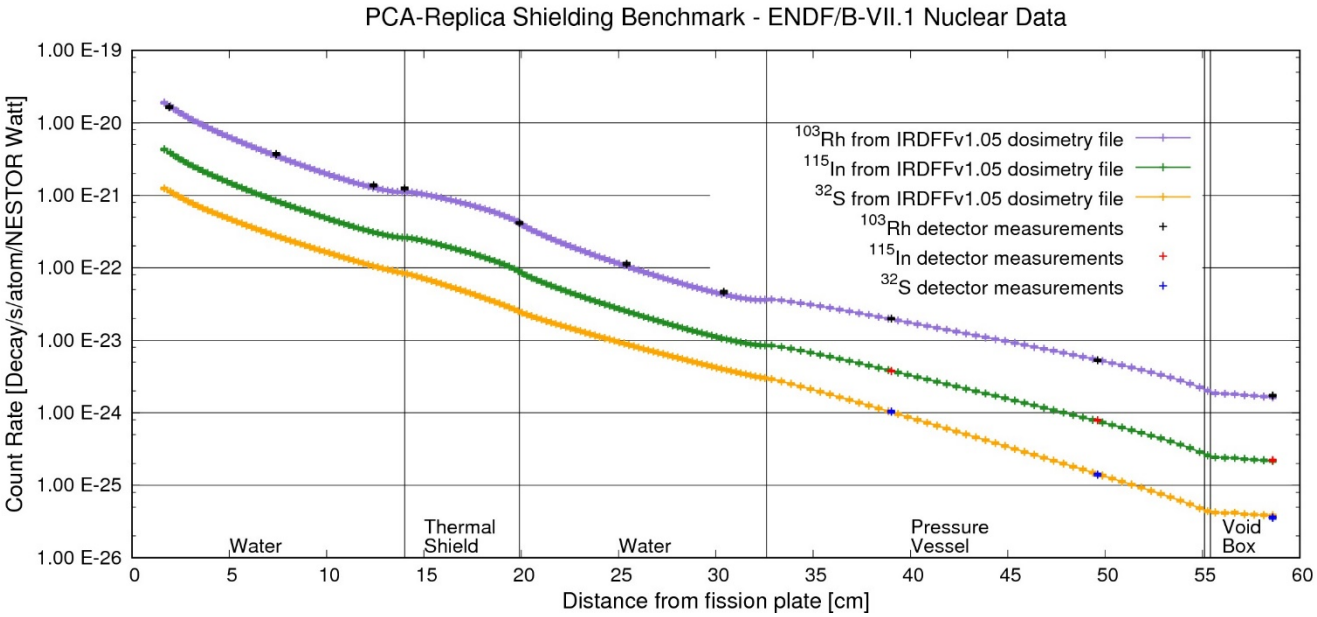

Figure D.E7.5. Dosimeter reaction-rate ENDF/B-VII.1 with IRDFFv1.05

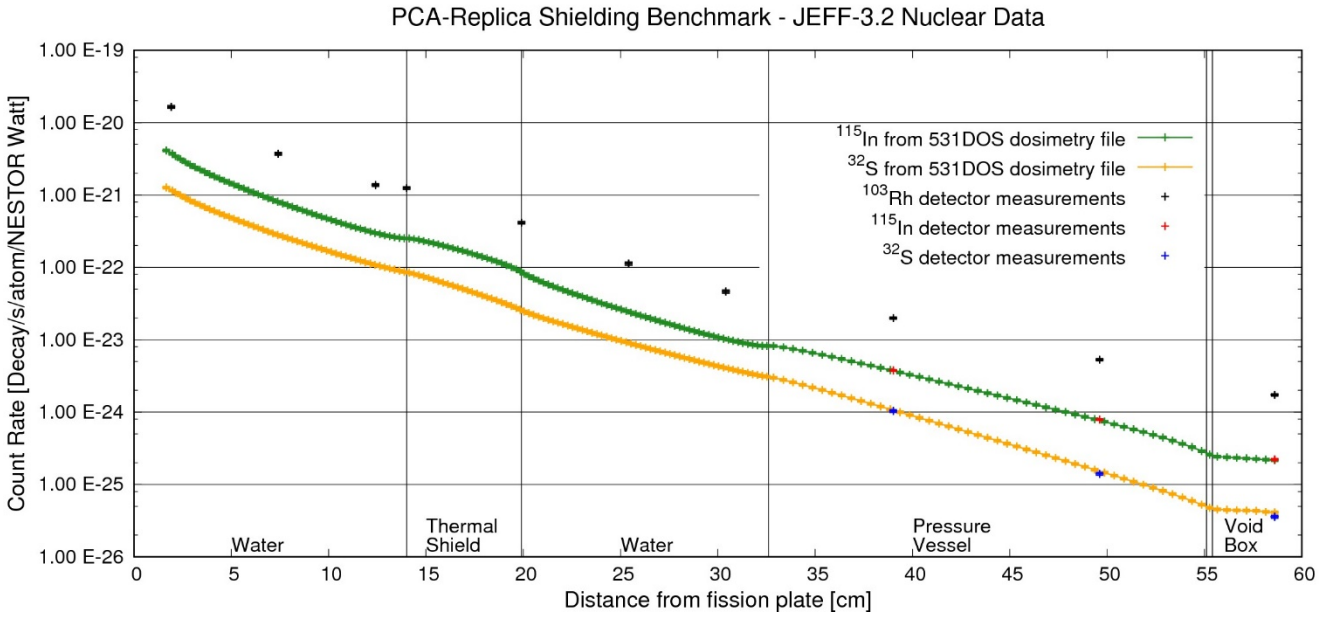

Figure D.JF32.1. Dosimeter reaction-rate JEFF-3.2 with 531DOS

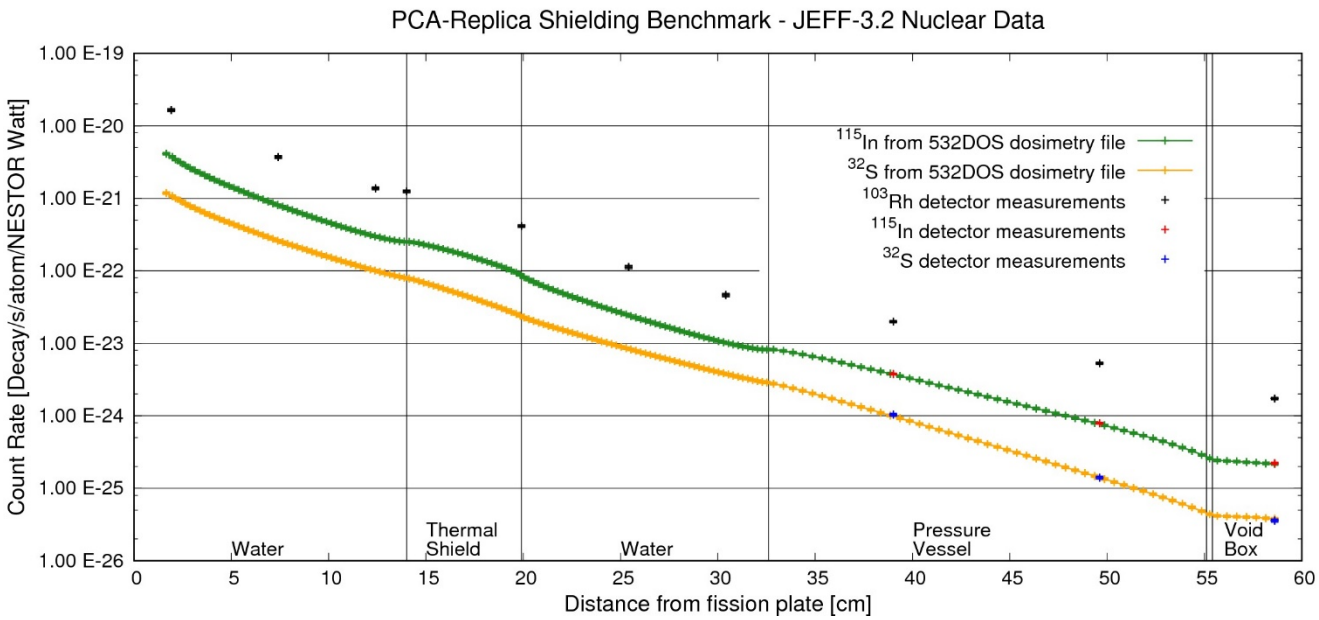

Figure D.JF32.2. Dosimeter reaction-rate JEFF-3.2 with 532DOS

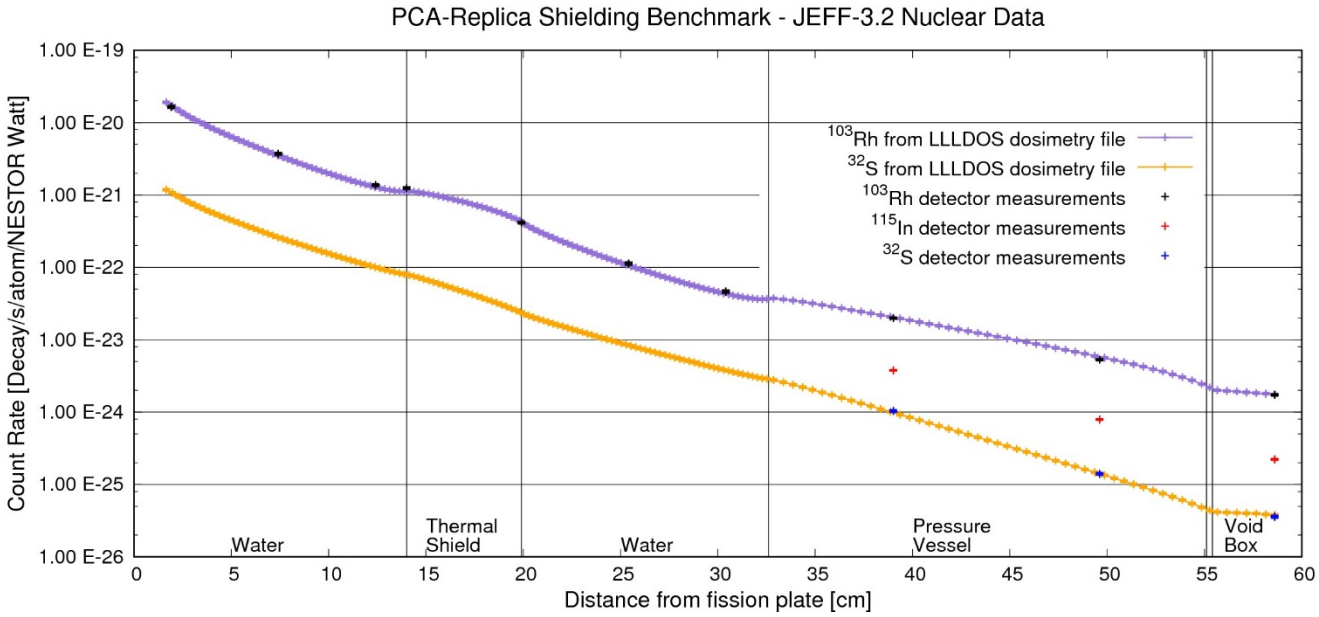

Figure D.JF32.3. Dosimeter reaction-rate JEFF-3.2 with LLLDOS

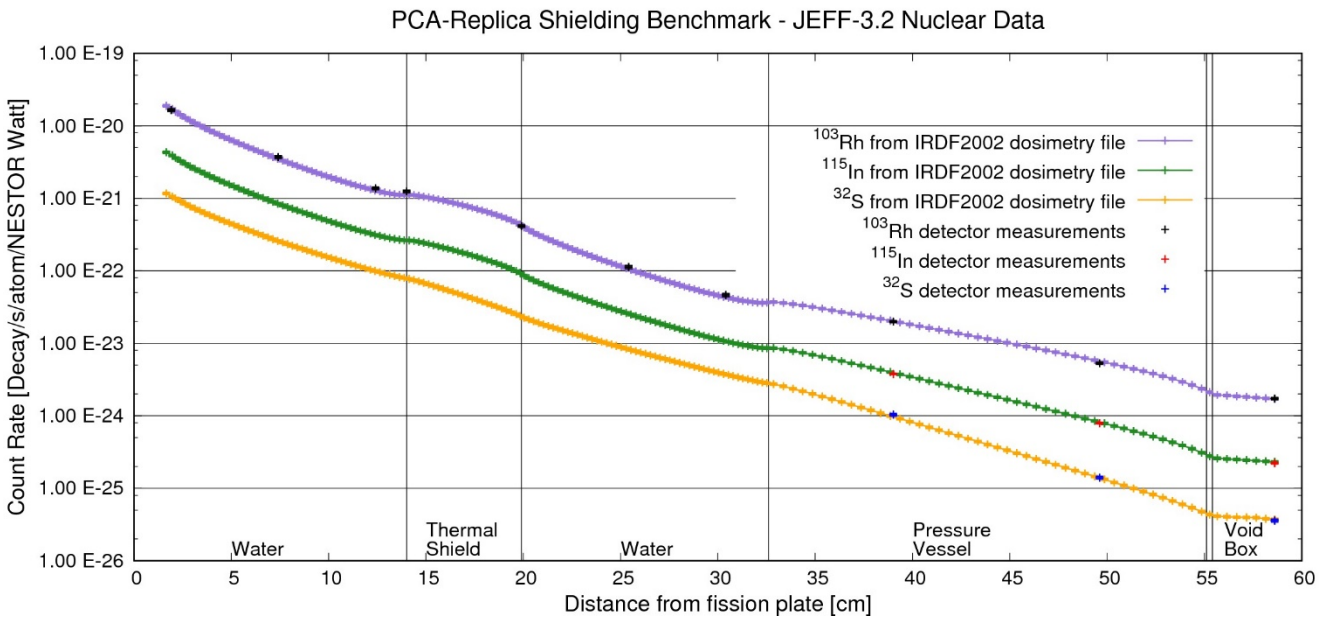

Figure D.JF32.4. Dosimeter reaction-rate JEFF-3.2 with IRDF2002

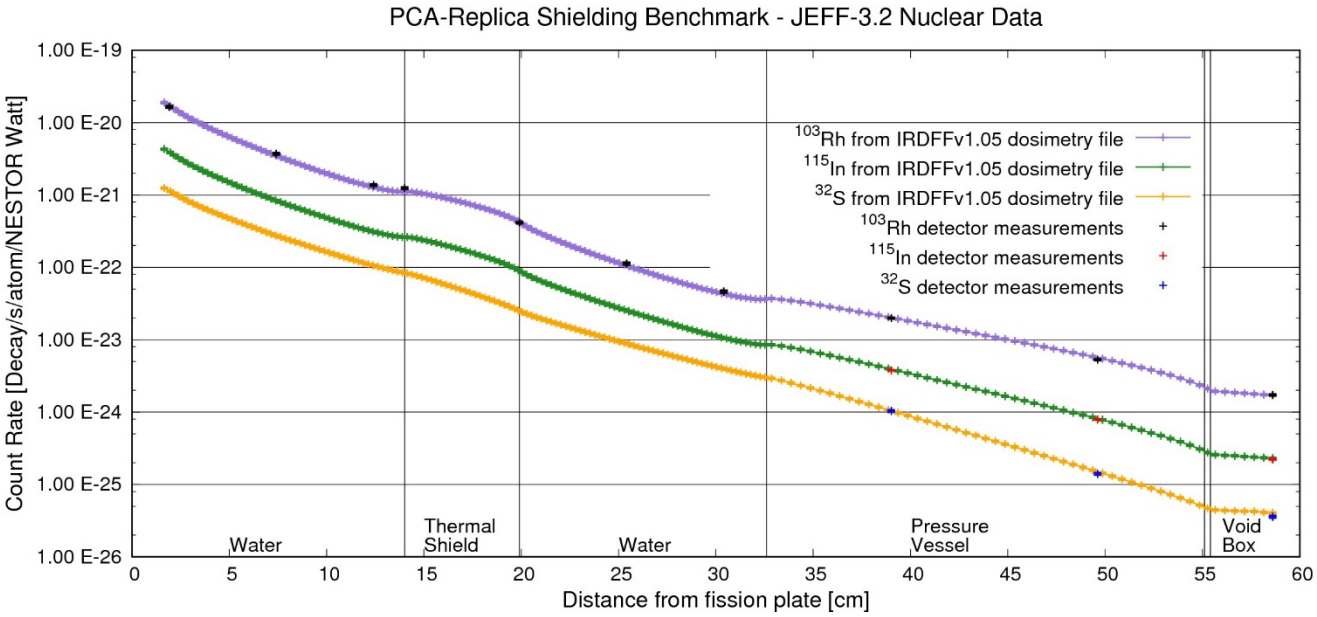

Figure D.JF32.5. Dosimeter reaction-rate JEFF-3.2 with IRDFFv1.05

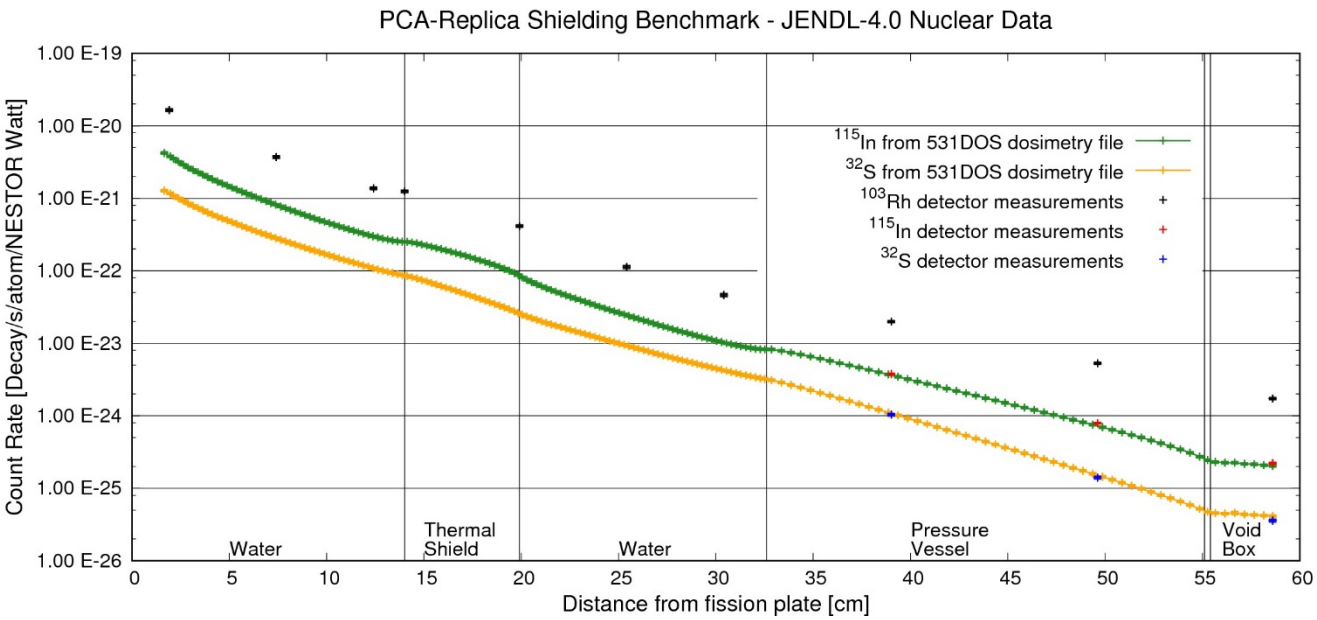

Figure D.JL4.1. Dosimeter reaction-rate JENDL-4.0 with 531DOS

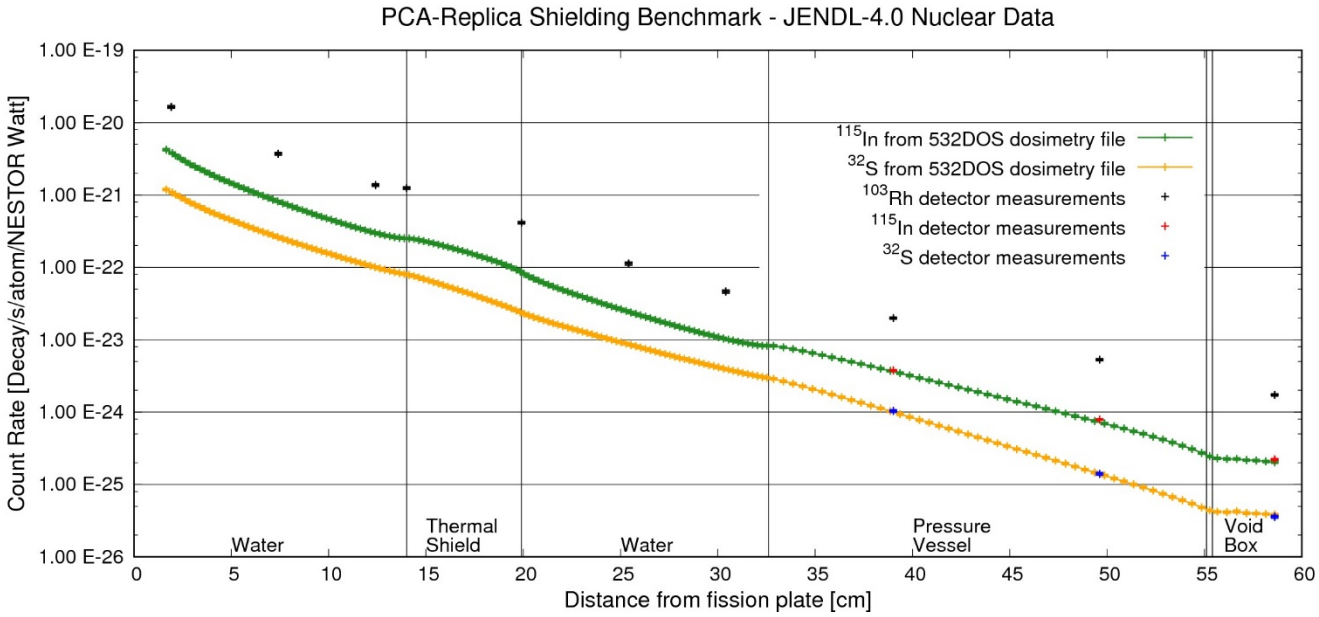

Figure D.JL4.2. Dosimeter reaction-rate JENDL-4.0 with 532DOS

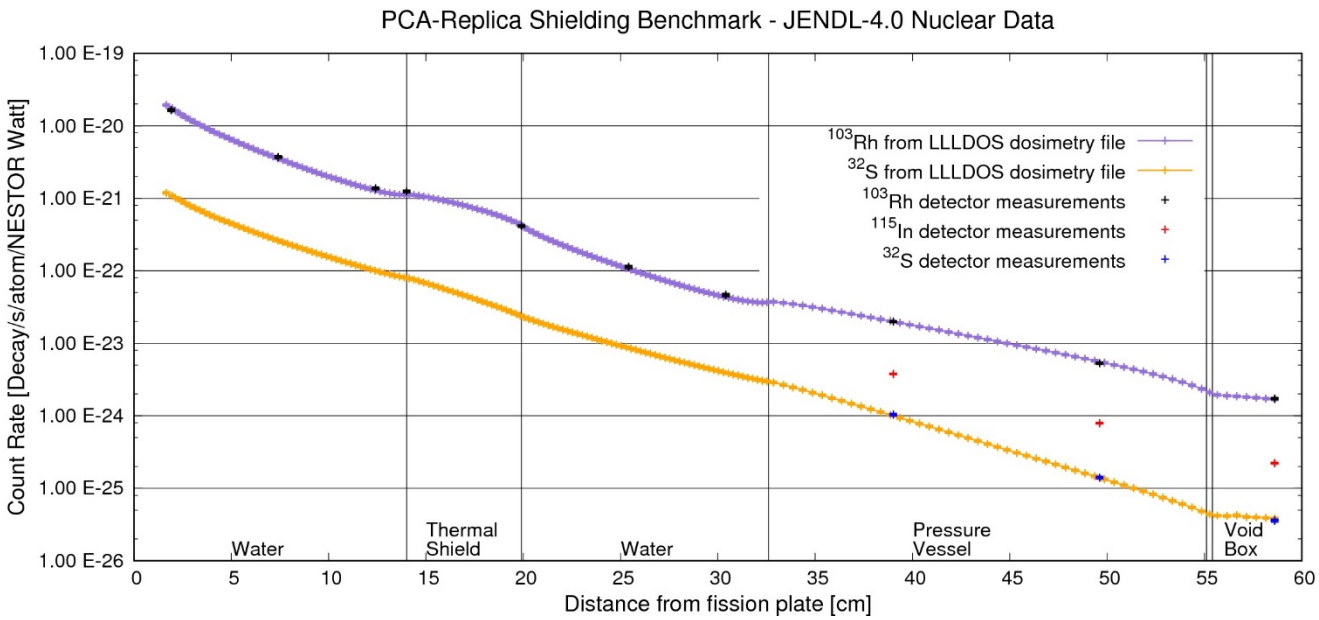

Figure D.JL4.3. Dosimeter reaction-rate JENDL-4.0 with LLLDOS

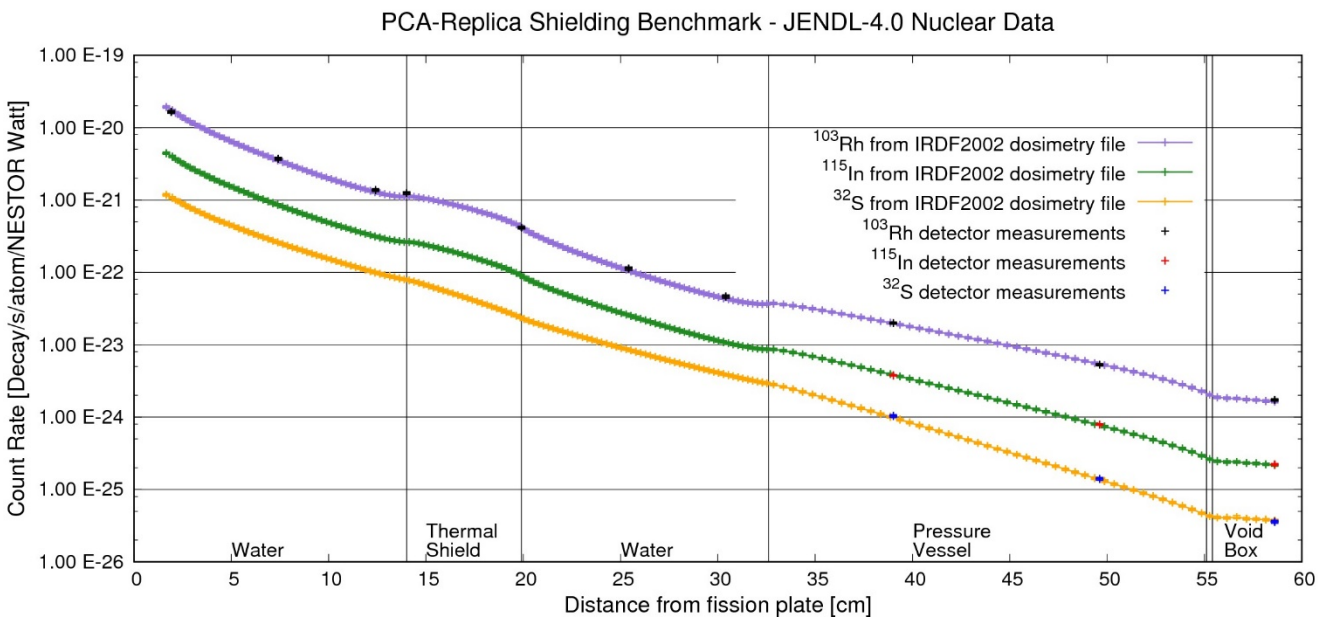

Figure D.JL4.4. Dosimeter reaction-rate JENDL-4.0 with IRDF2002

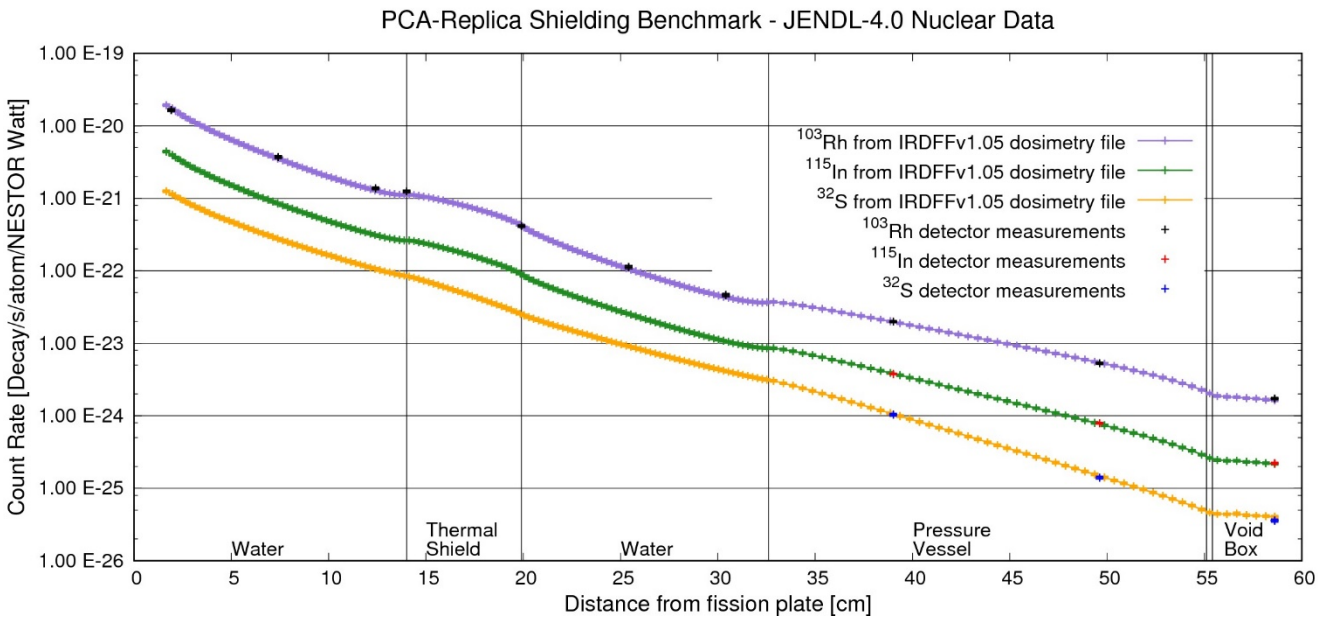

Figure D.JL4.5. Dosimeter reaction-rate JENDL-4.0 with IRDFFv1.05

To look more closely at the comparison, in the following DR series of eighteen Figures we present the (Dosimeter) Ratio of the calculated value related to the measurements (i.e. C/E values). Error bars in these Figures are 1 standard deviation and include both calculation and measurement errors.

Figs. DR.In.1, DR.In.2, DR.In.3, DR.In.4, DR.In.5 and DR.In.6 show the C/E Dosimeter Ratios for all existing dosimetry files for the ^{115}In(n,n')^{115m}In dosimeters for the ENDF-B/VI.6, ENDF/B-VII.1, JEFF-3.1, JEFF-3.1.2, JEFF-3.2 and JENDL-4.0 transport libraries respectively. Similarly Figs. DR.Rh.1 – DR.Rh.6 show the C/E Dosimeter Ratios for all existing dosimetry files for the ^{103}Rh(n,n')^{103m}Rh dosimeters for the same transport library set and Figs. DR.S.1 – DR.S.6 show the

C/E Dosimeter Ratios for all existing dosimetry files for the $^{32}S(n,p)^{32}P$ dosimeters again for the same transport library set.

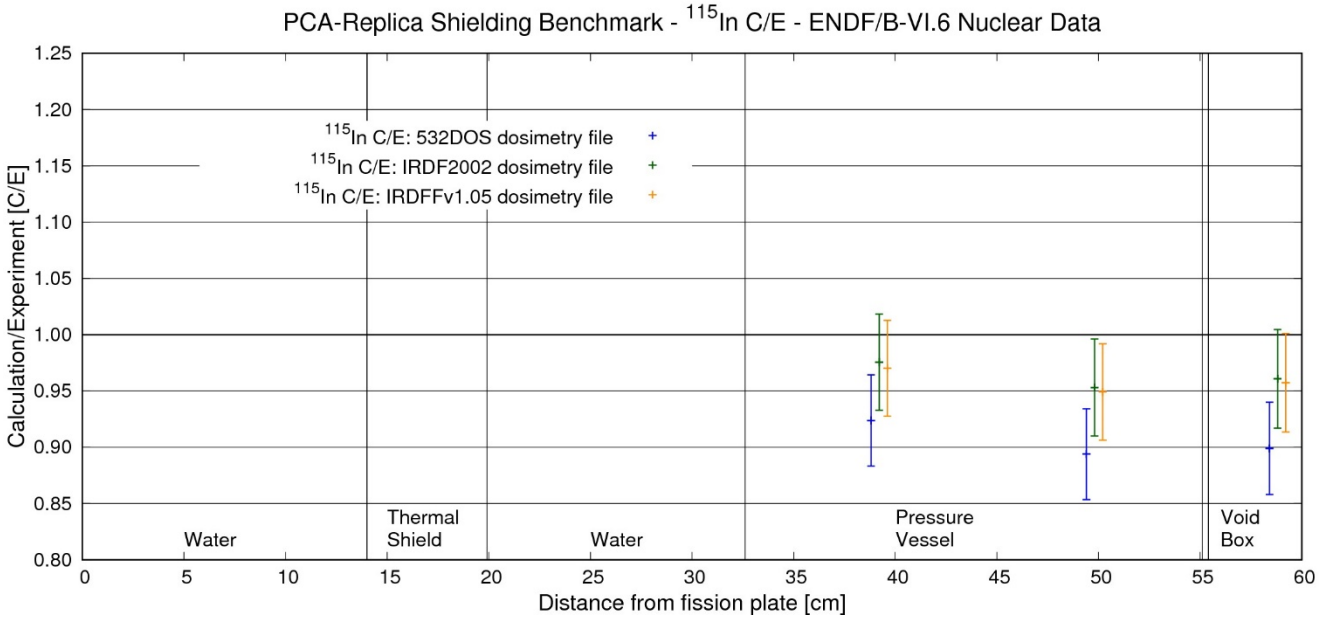

Figure DR.In.1. Ratio of Calculation to Experiment for ^{115}In and ENDF/B-VI.6

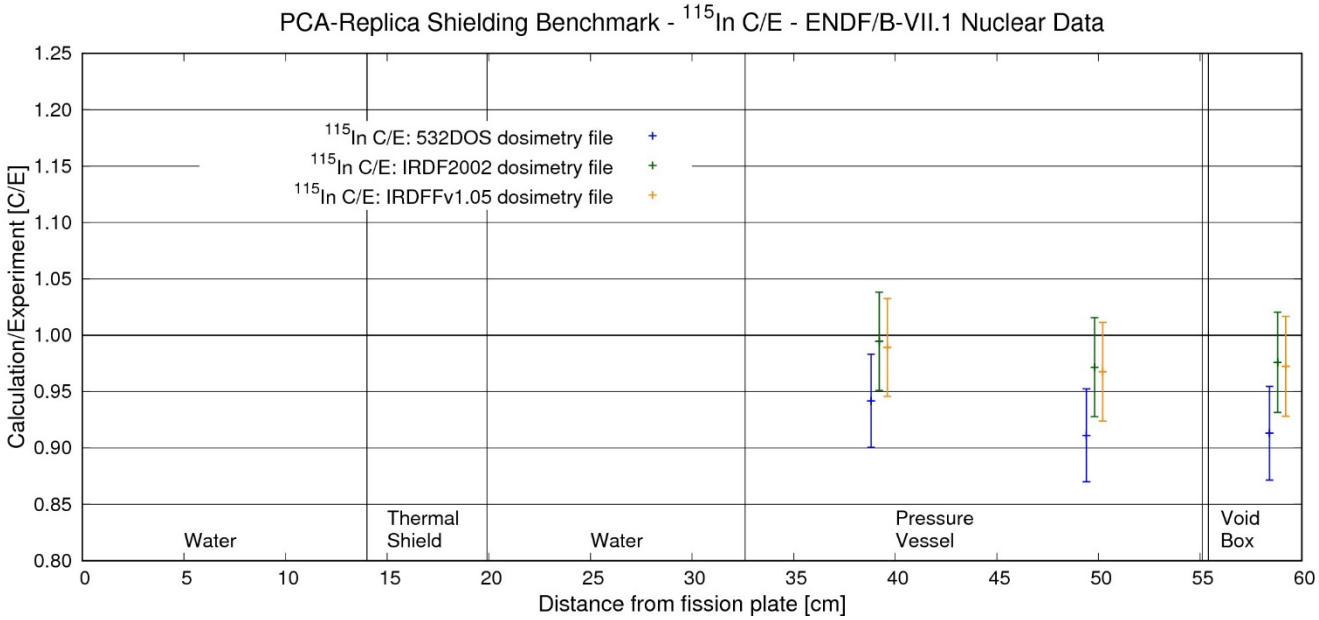

Figure DR.In.2. Ratio of Calculation to Experiment for ^{115}In and ENDF/B-VII.1

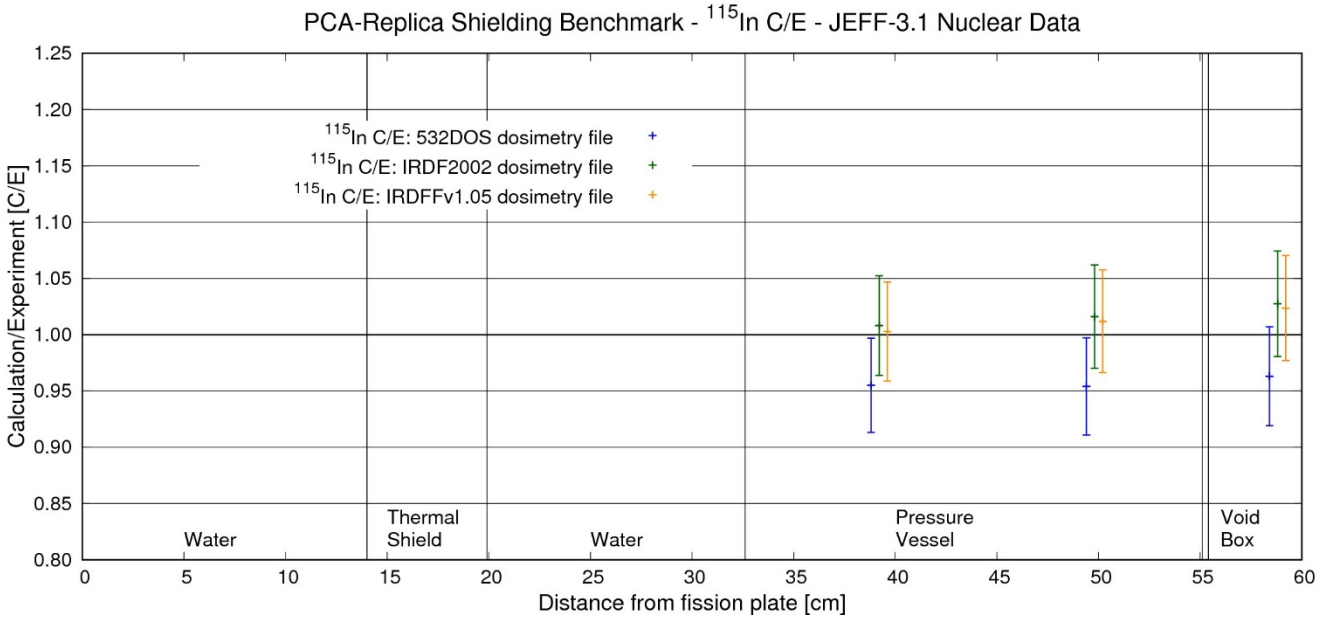

Figure DR.In.3. Ratio of Calculation to Experiment for ^{115}In and JEFF-3.1

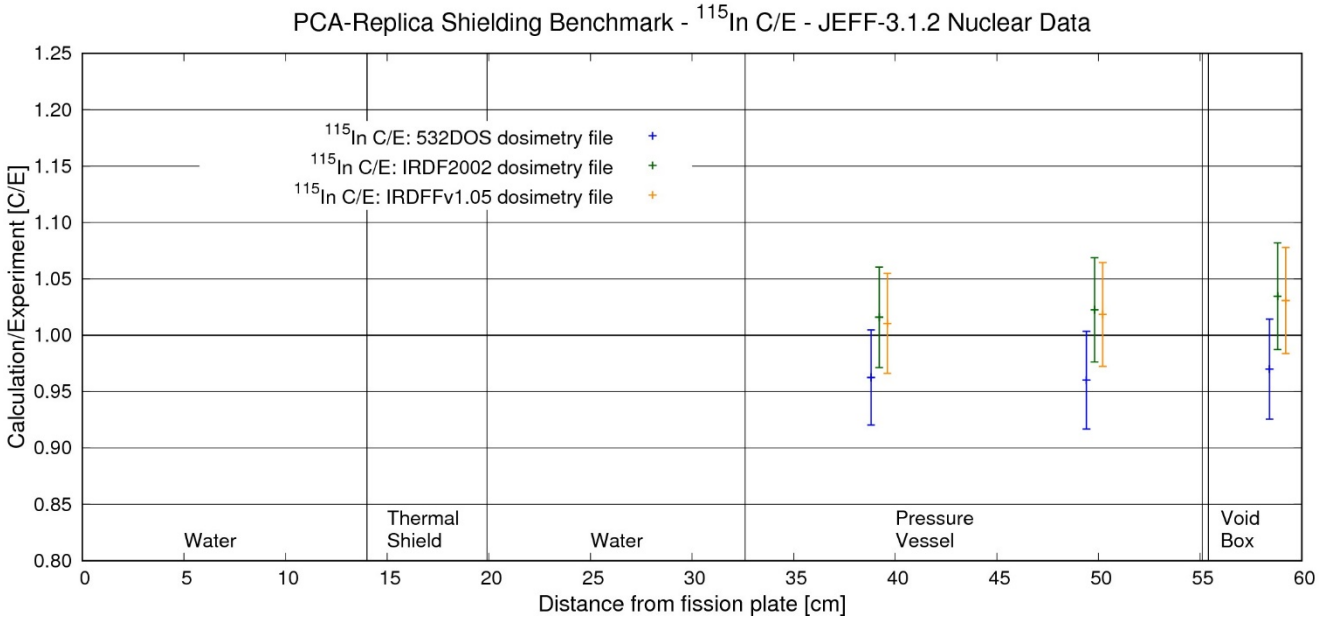

Figure DR.In.4. Ratio of Calculation to Experiment for ^{115}In and JEFF-3.1.2

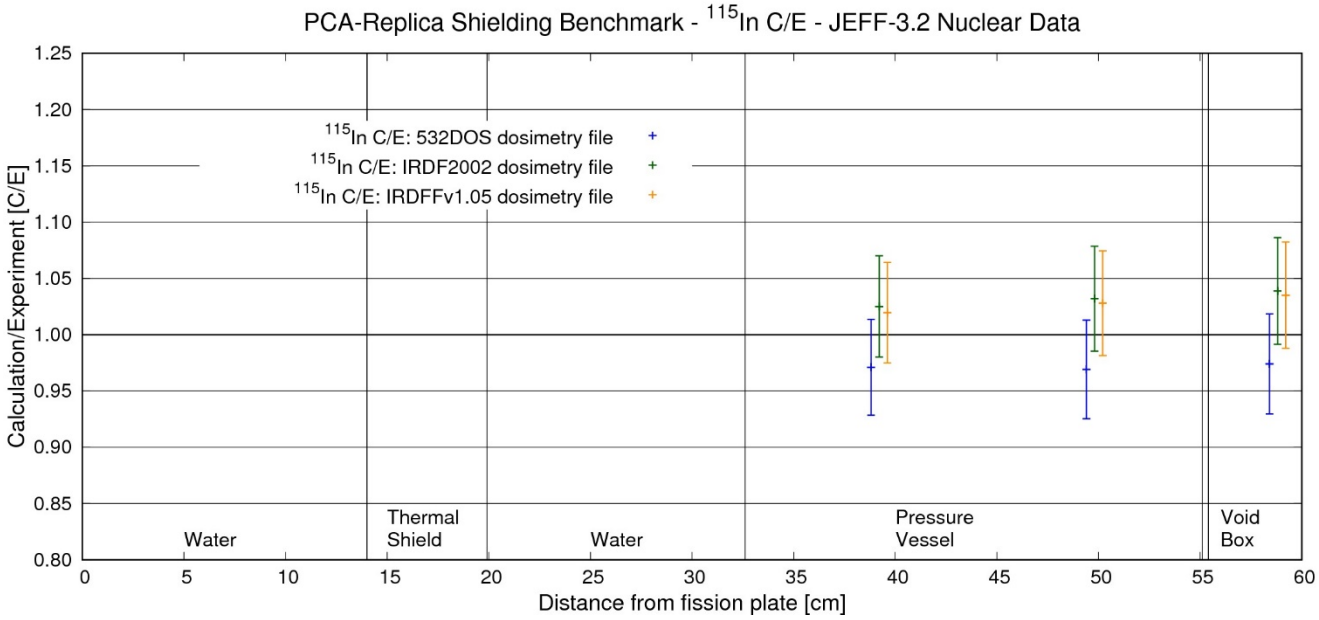

Figure DR.In.5. Ratio of Calculation to Experiment for ^{115}In and JEFF-3.2

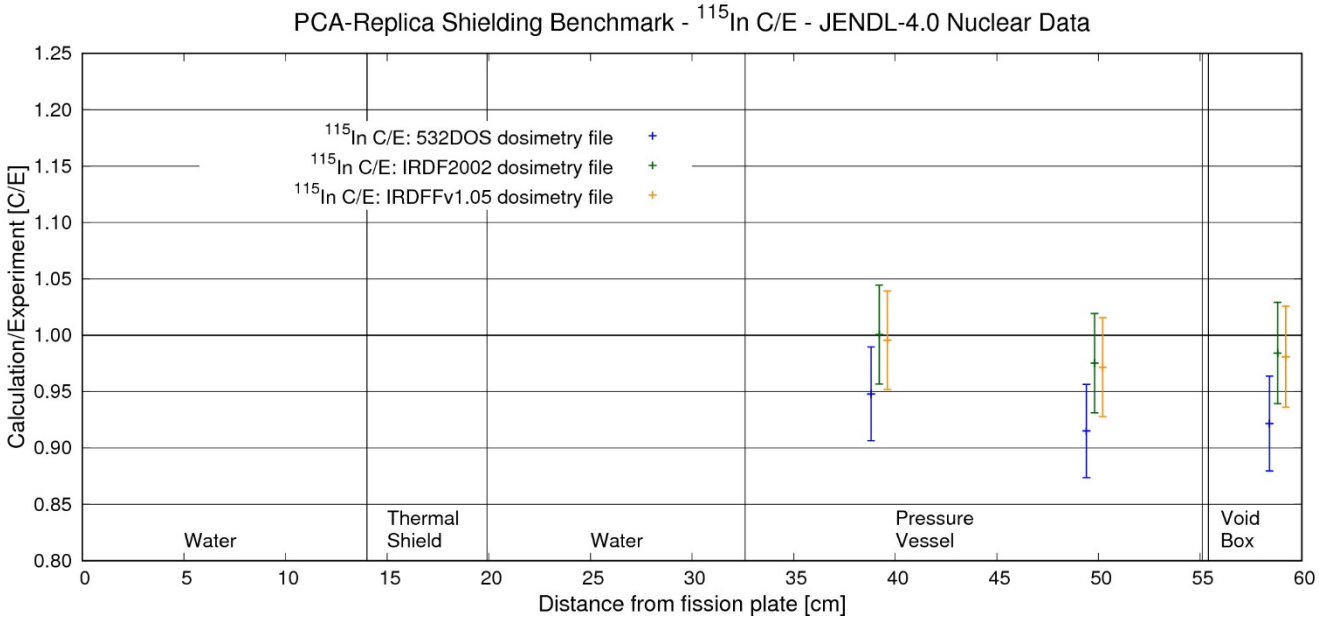

Figure DR.In.6. Ratio of Calculation to Experiment for ^{115}In and JENDL-4.0

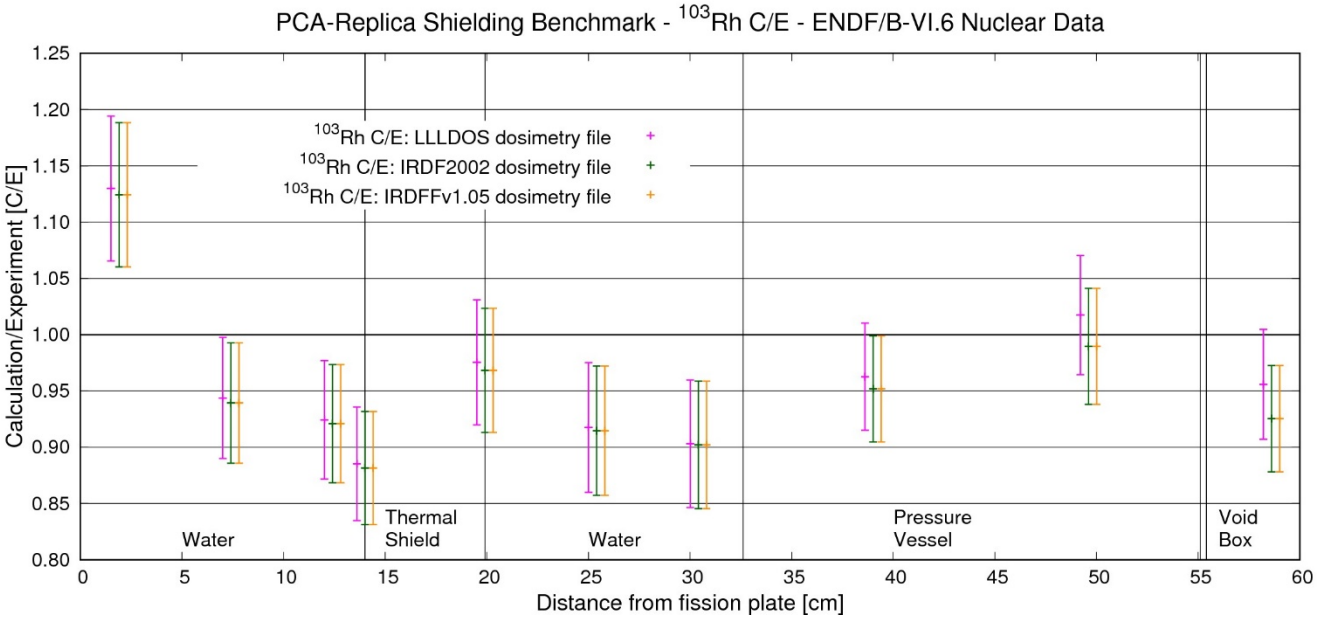

Figure DR.Rh.1. Ratio of Calculation to Experiment for ^{103}Rh and ENDF/B-VI.6

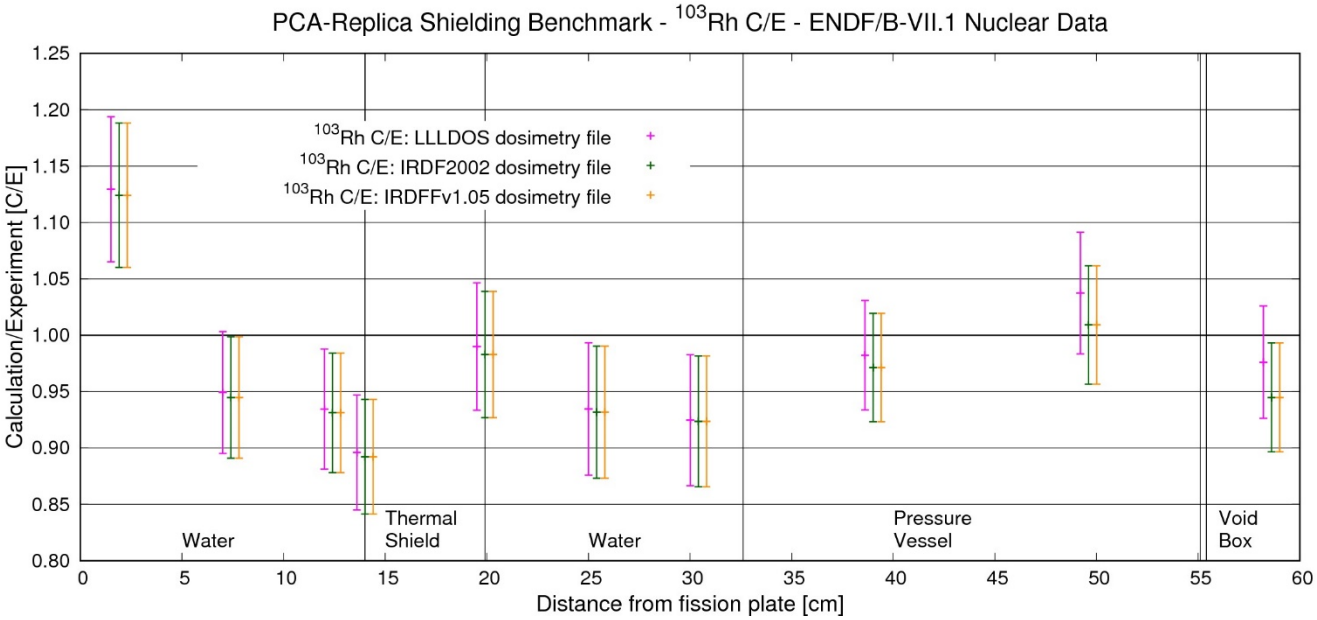

Figure DR.Rh.2. Ratio of Calculation to Experiment for ^{103}Rh and ENDF/B-VII.1

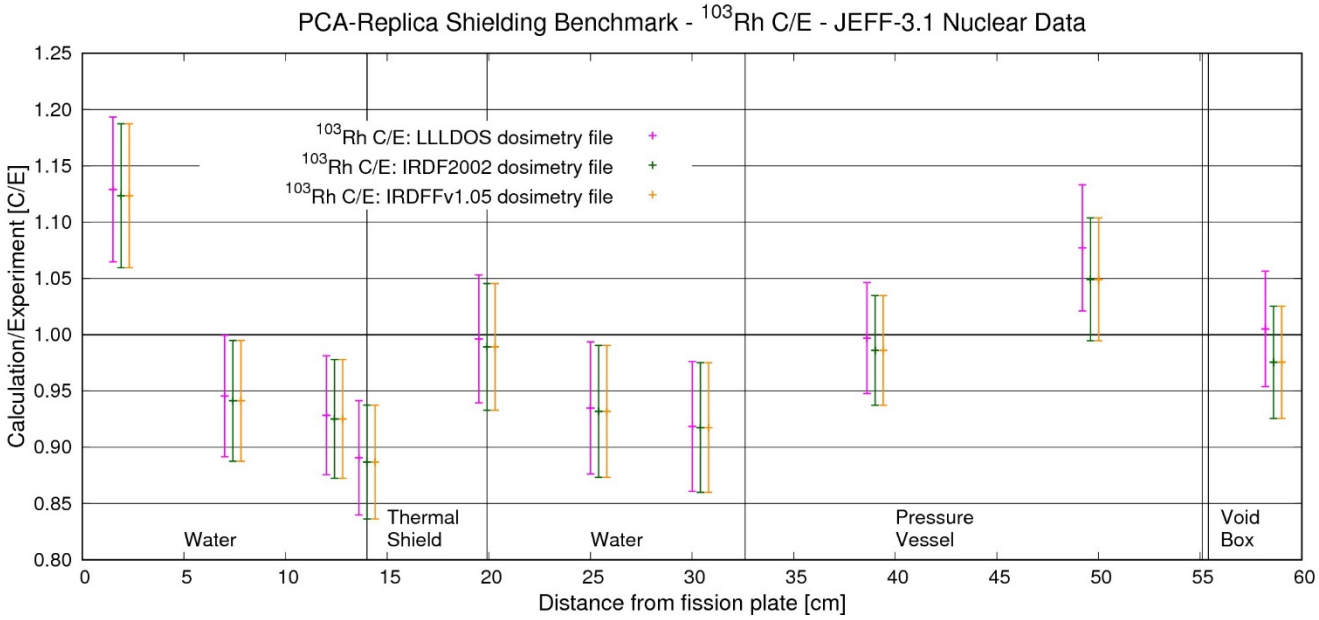

Figure DR.Rh.3. Ratio of Calculation to Experiment for ^{103}Rh and JEFF-3.1

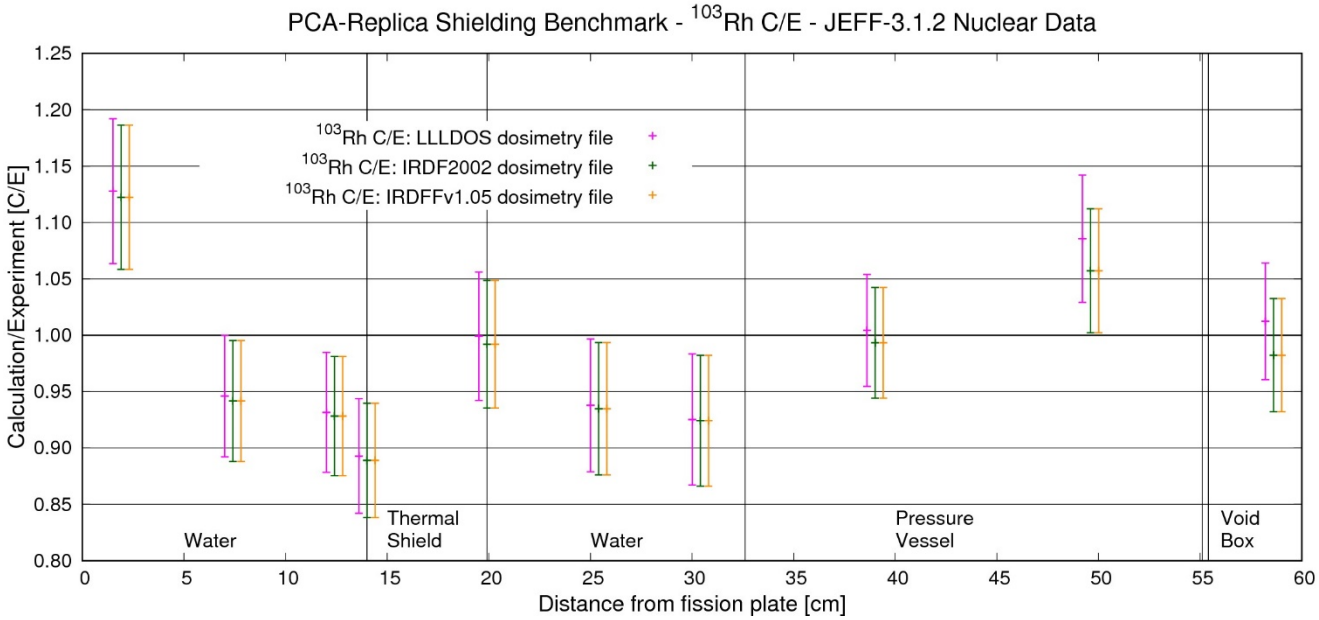

Figure DR.Rh.4. Ratio of Calculation to Experiment for ^{103}Rh and JEFF-3.1.2

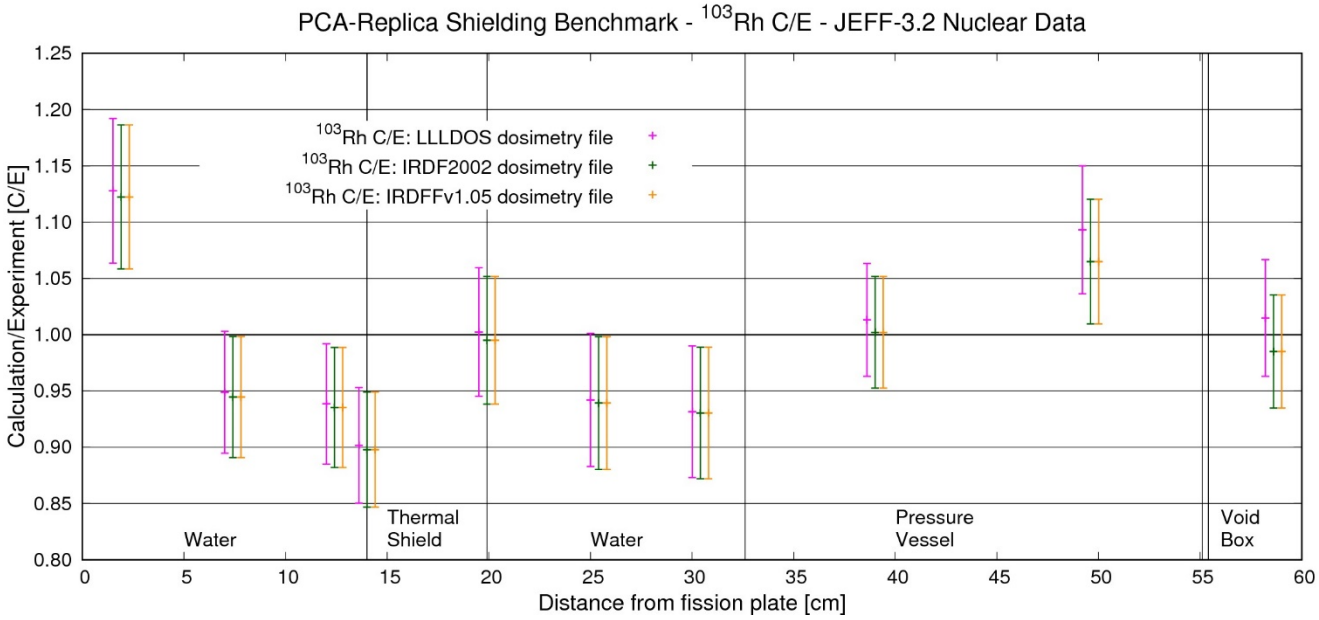

Figure DR.Rh.5. Ratio of Calculation to Experiment for ^{103}Rh and JEFF-3.2

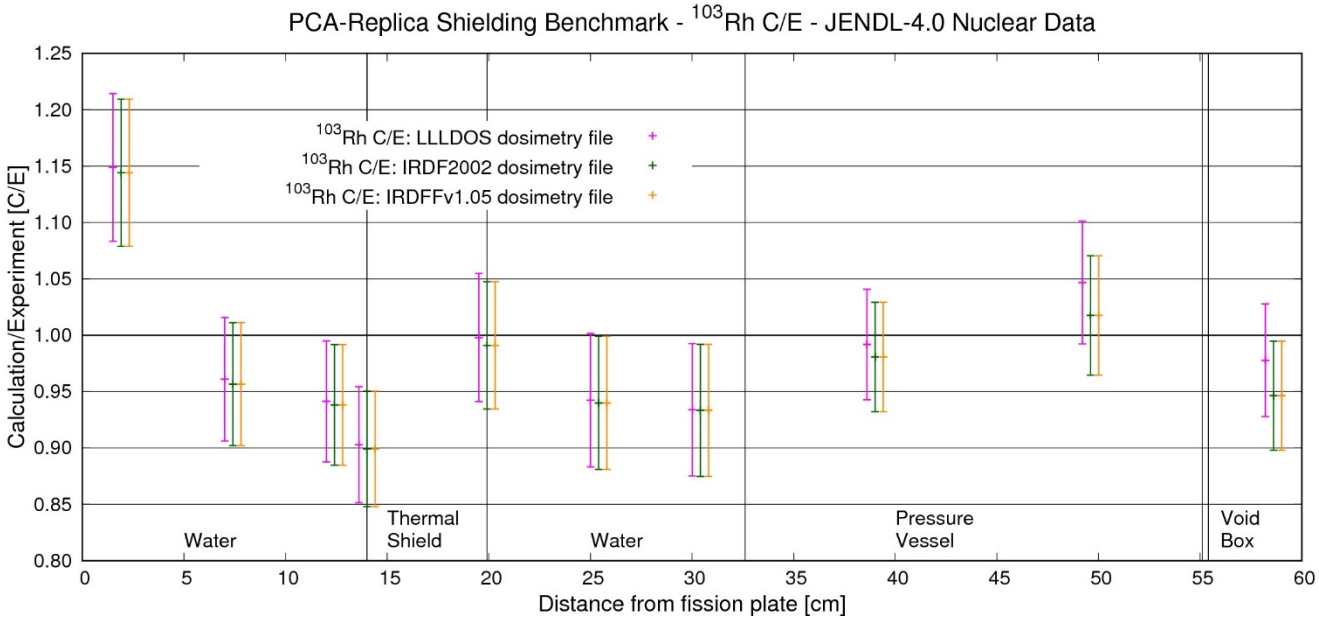

Figure DR.Rh.6. Ratio of Calculation to Experiment for ^{103}Rh and JENDL-4.0

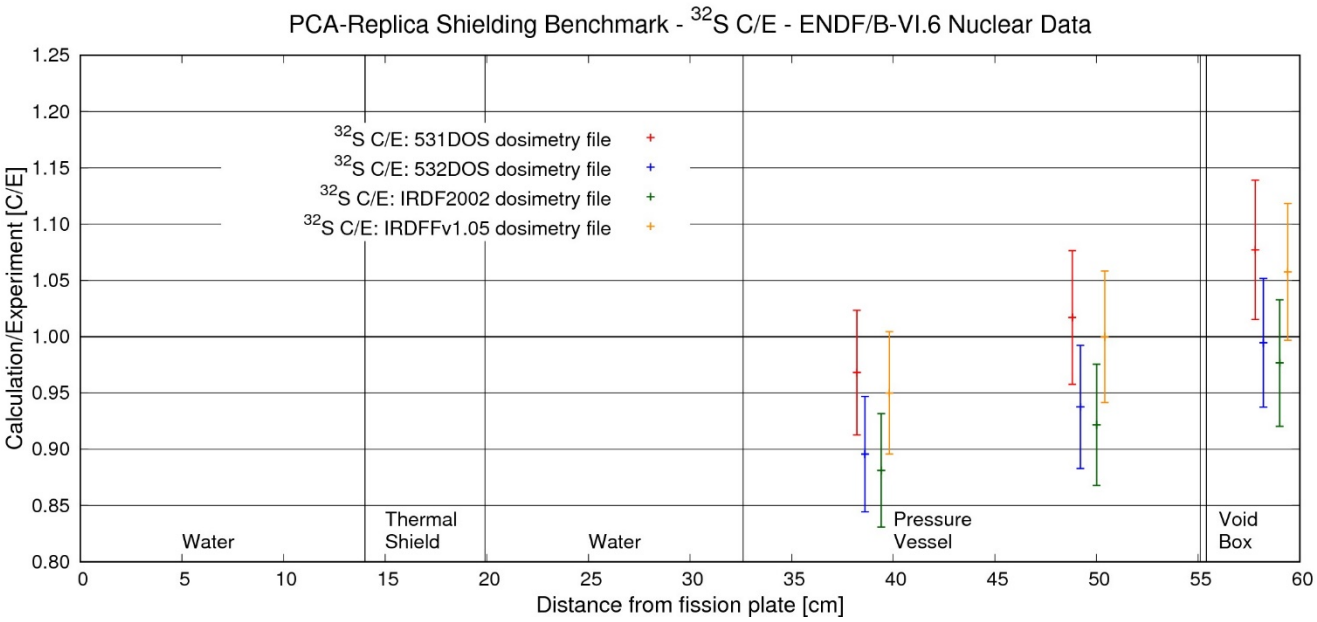

Figure DR.S.1. Ratio of Calculation to Experiment for ^{32}S and ENDF/B-VI.6

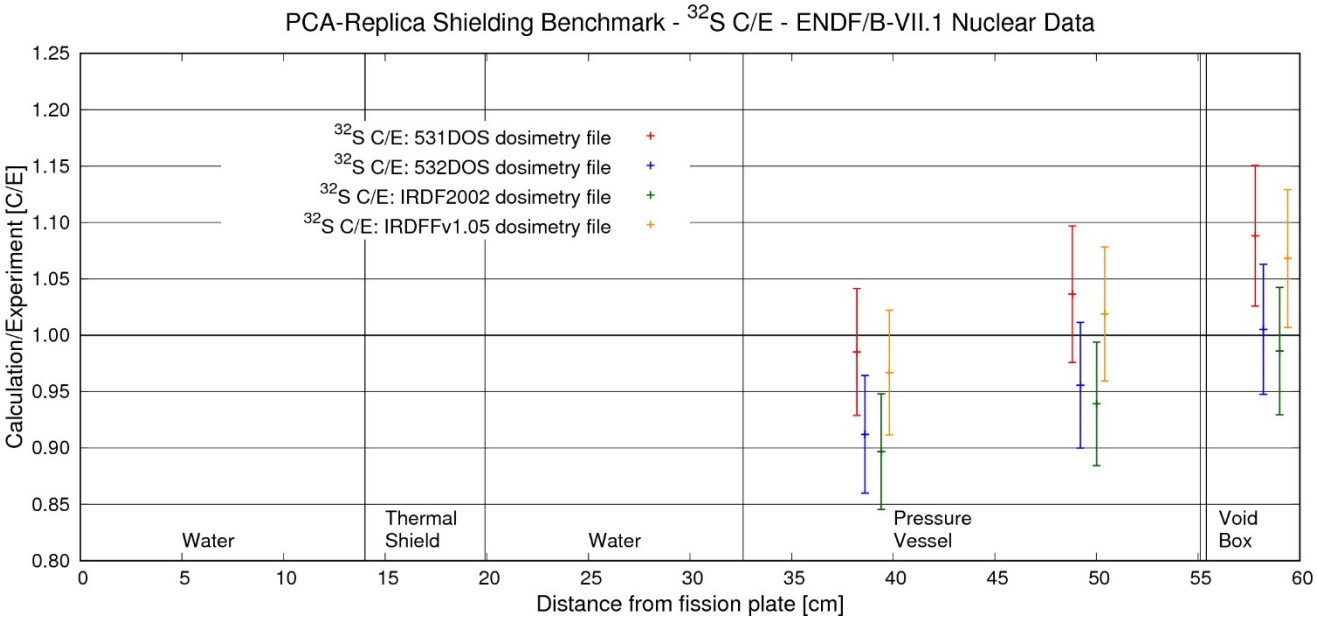

Figure DR.S.2. Ratio of Calculation to Experiment for ^{32}S and ENDF/B-VII.1

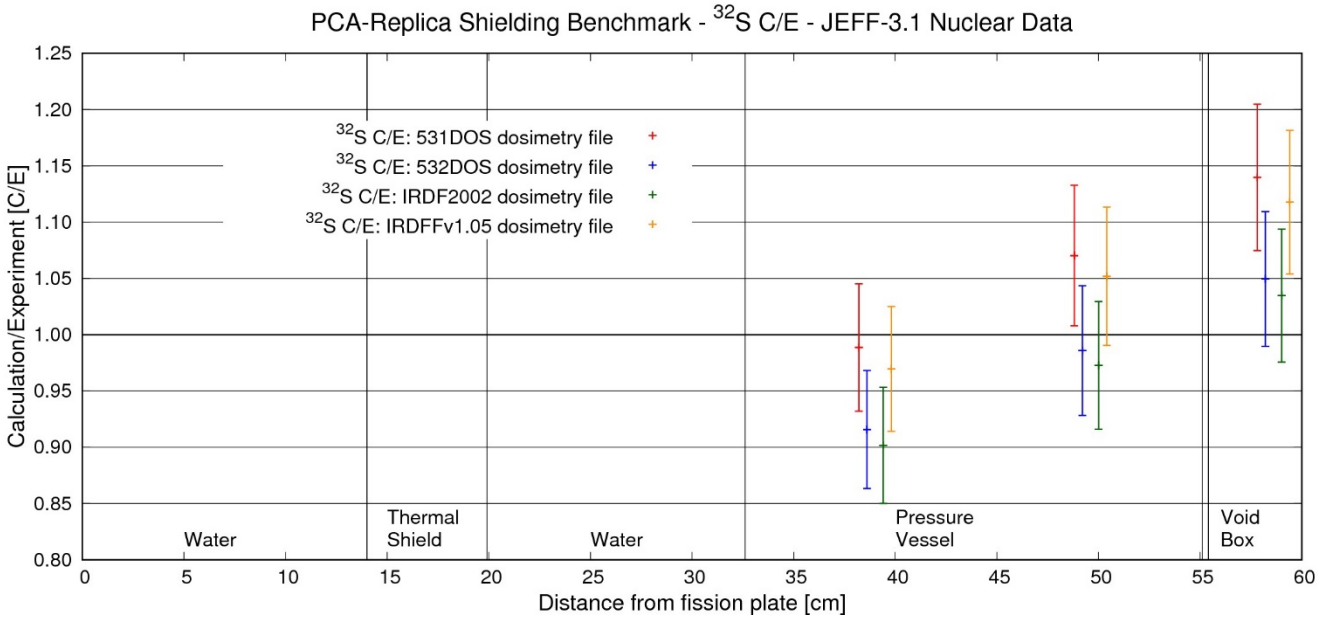

Figure DR.S.3. Ratio of Calculation to Experiment for ^{32}S and JEFF-3.1

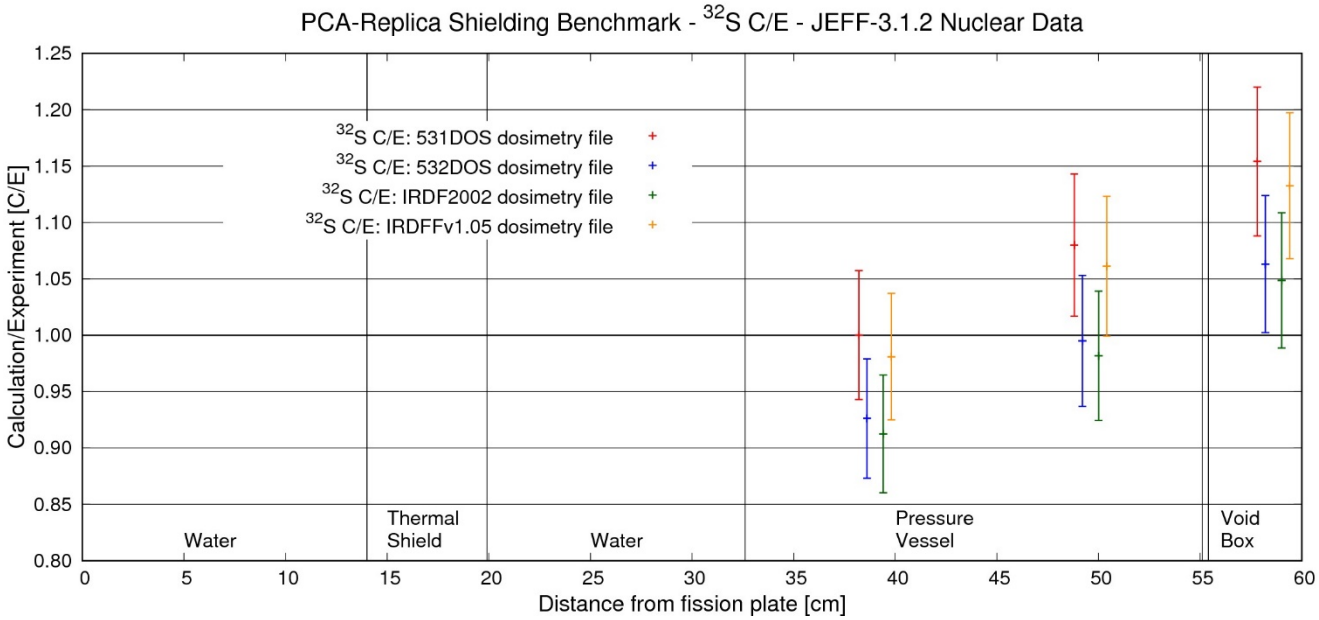

Figure DR.S.4. Ratio of Calculation to Experiment for ^{32}S and JEFF-3.1.2

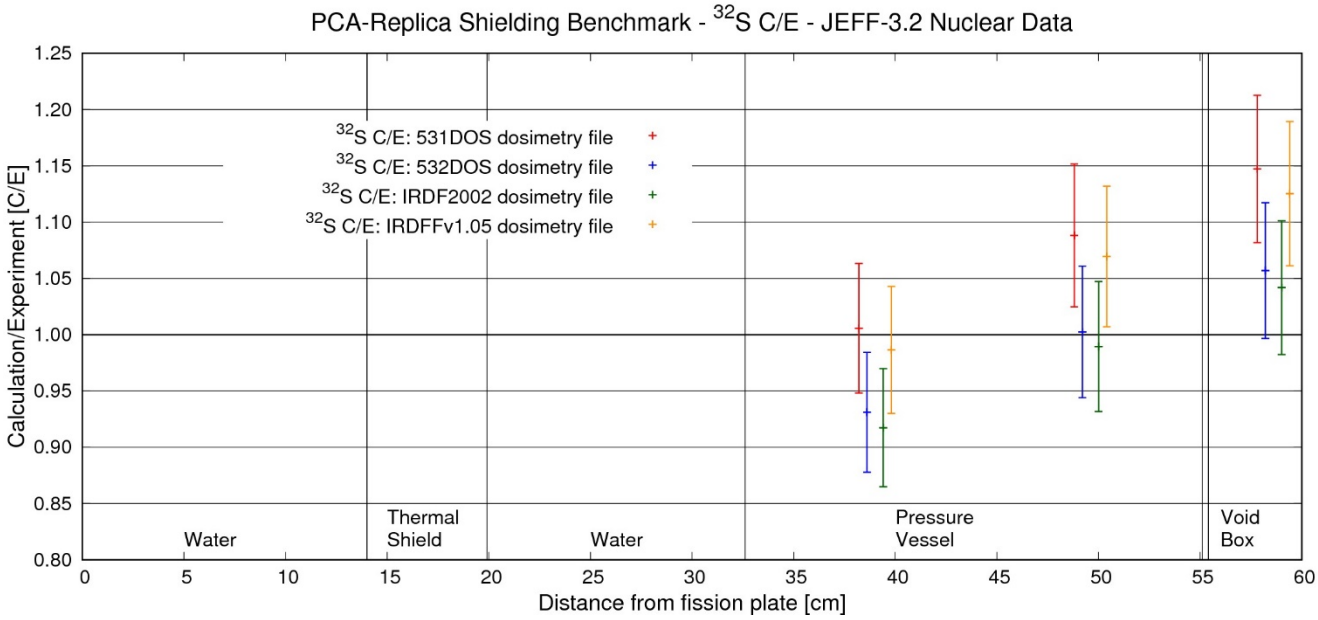

Figure DR.S.5. Ratio of Calculation to Experiment for ^{32}S and JEFF-3.2

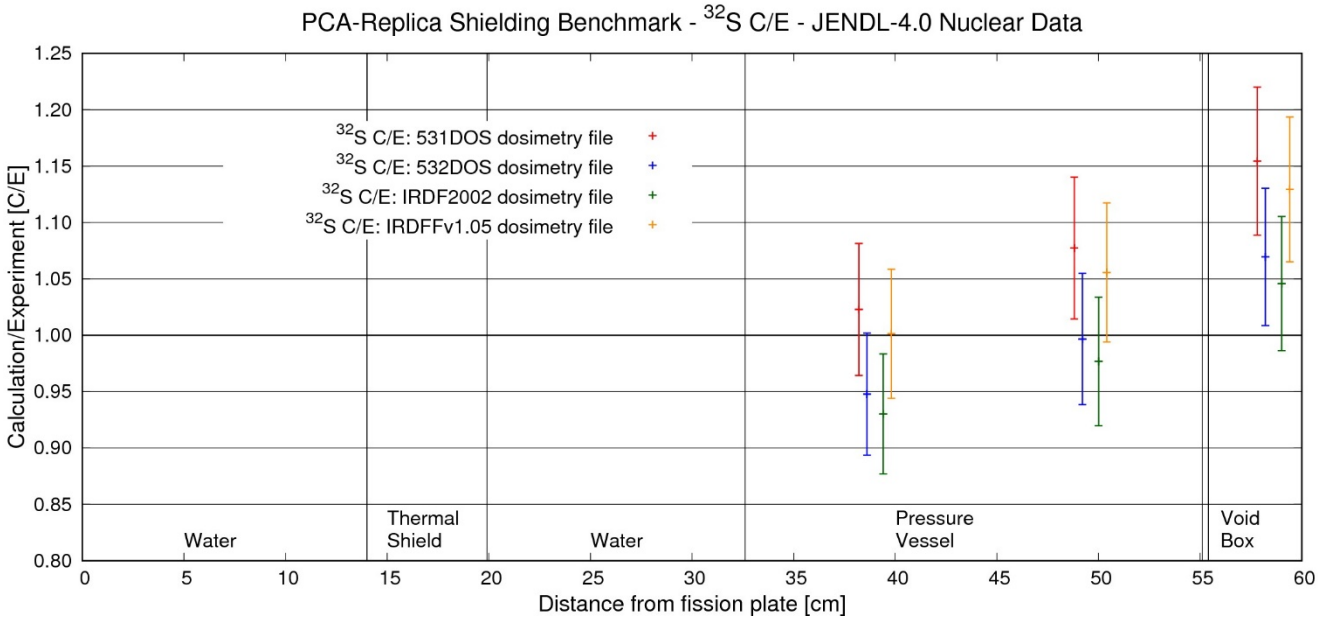

Figure DR.S.6. Ratio of Calculation to Experiment for ^{32}S and JENDL-4.0

Calculated and measured (unfolded) neutron spectra were compared for the positions of dosimeters 8 and 10. The lowest of the 42 energy groups in Table 6 was excluded due to too high statistical uncertainties on the calculated flux. The uncertainties on each of the remaining 41 energy group fluxes, although as expected higher than those on the detector responses (below 1% as discussed in §7), were still in the main satisfactory, given also that the uncertainty in the source intensity (§5) is 3.8%. In particular, for position 8, the average Monte Carlo error over all 6 data libraries and all 41 energy groups was 0.6% with a maximum of 7.2% (JENDL-4.0, 67 - 76 keV). Instead for position 10, the average error over all 6 data libraries and all 41 energy groups was 1.8% with a maximum of 23.6% (JEFF-3.1, 76 - 86 keV). Figs. S.PV.1, S.PV.2, S.PV.3, S.PV.4, S.PV.5 and S.PV.6 show the calculated

and measured Spectra at dosimeter position 8 (i.e. in the PV sample) for ENDF-B/VI.6, ENDF/B-VII.1, JEFF-3.1, JEFF-3.1.2, JEFF-3.2 and JENDL-4.0 transport libraries respectively. Similarly, Figs. S.V.1 – S.V.6 show the calculated and measured Spectra at dosimeter position 10 (i.e. in the Void after the PV sample) for the same set of transport libraries. Again as for the dosimeter results the calculational results and measurements are completely independent of each other, each being normalized to the NESTOR power. Also the previously cited measurement errors and the stochastic calculational uncertainties are reported in these Figures, as 1 standard deviation error bars.

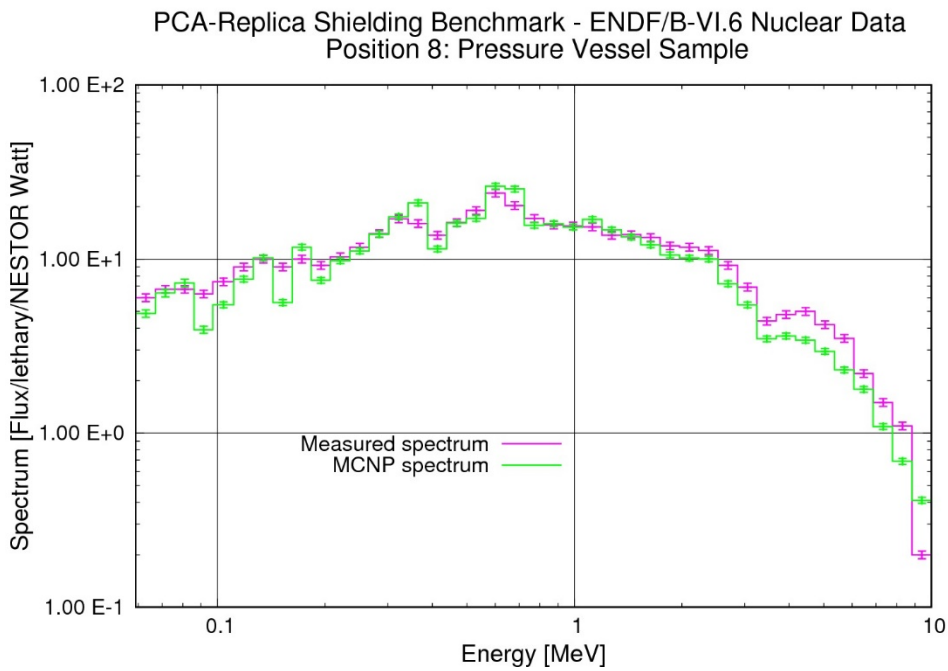

Figure S.PV.1. Calculation and Measured neutron spectra at position 8 – ENDF/B-VI.6

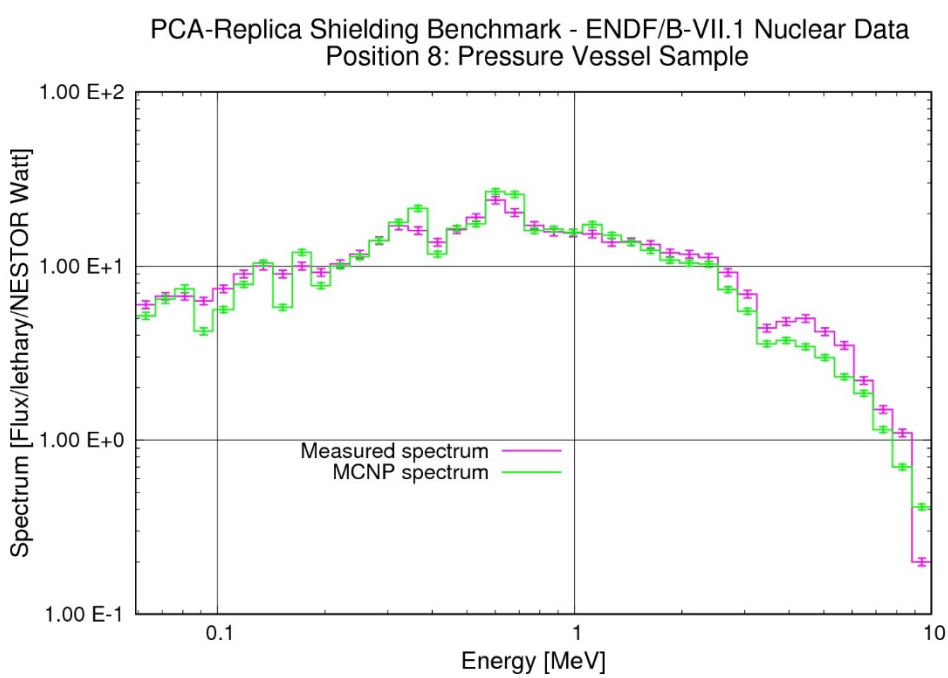

Figure S.PV.2. Calculation and Measured neutron spectra at position 8 – ENDF/B-VII.1

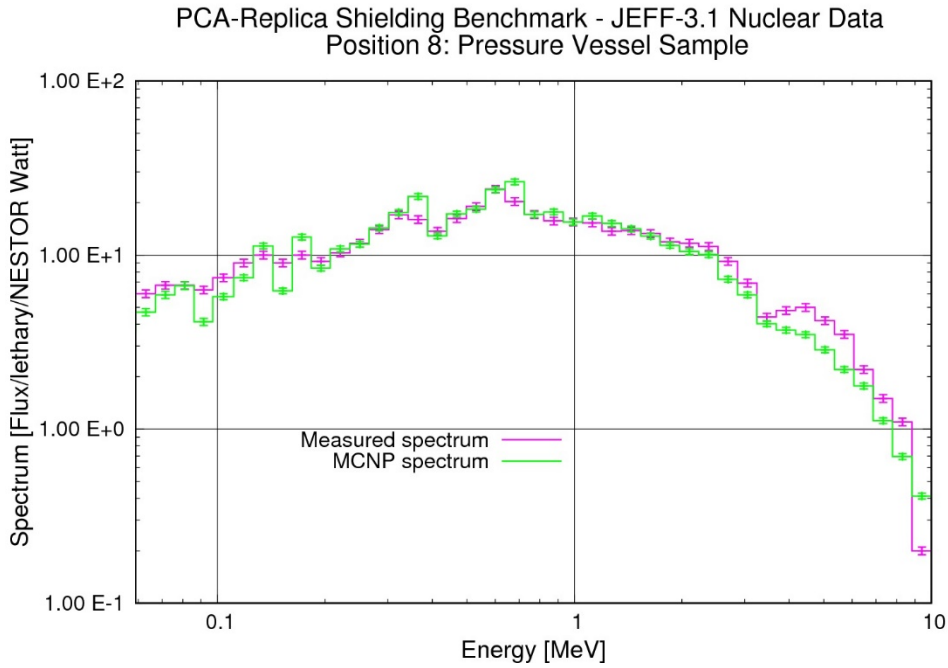

Figure S.PV.3. Calculation and Measured neutron spectra at position 8 – JEFF-3.1

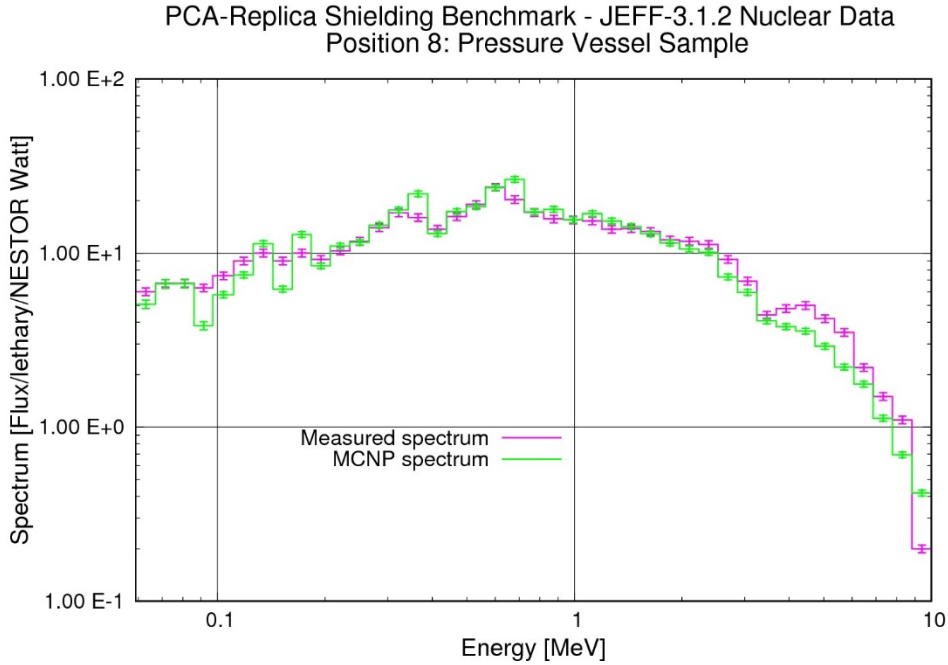

Figure S.PV.4. Calculation and Measured neutron spectra at position 8 – JEFF-3.1.2

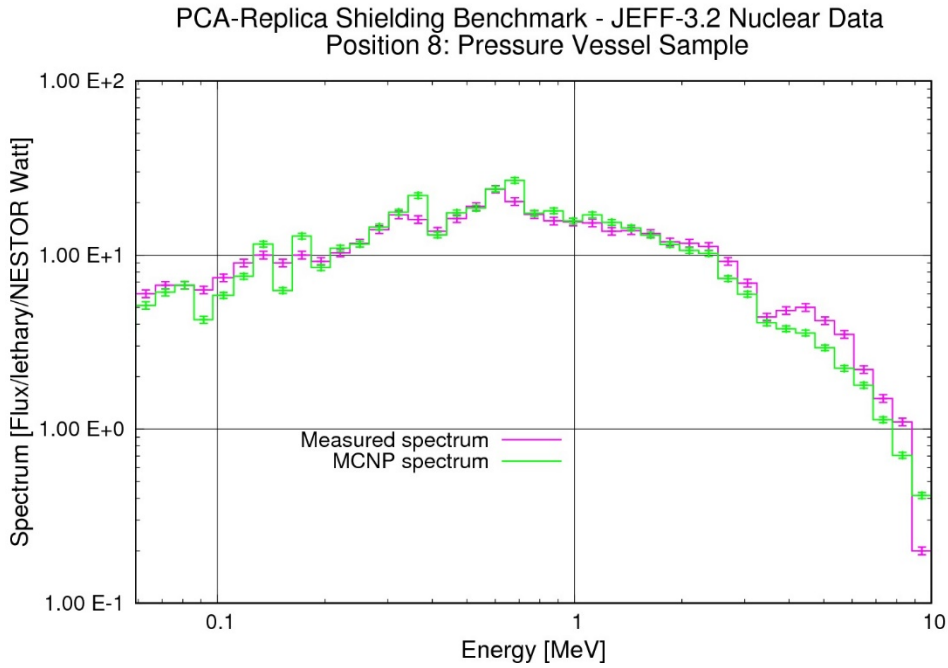

Figure S.PV.5. Calculation and Measured neutron spectra at position 8 – JEFF-3.2

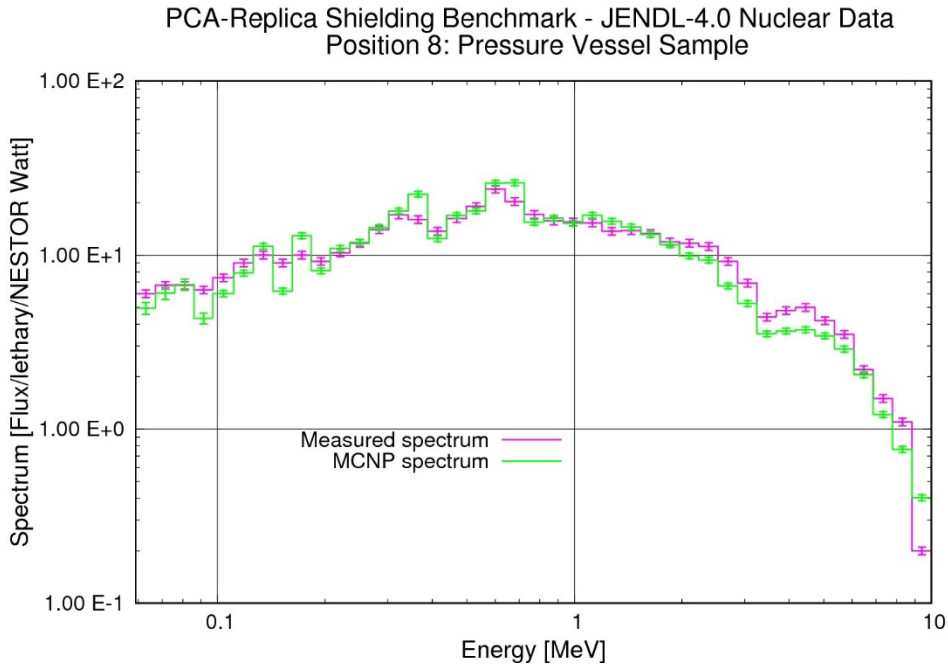

Figure S.PV.6. Calculation and Measured neutron spectra at position 8 – JENDL-4.0

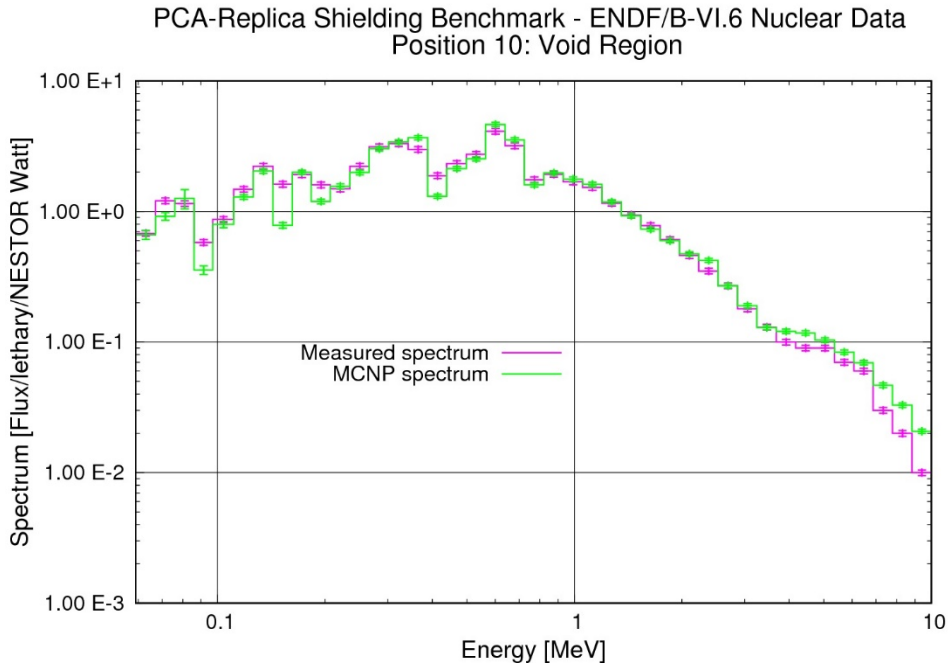

Figure S.V.1. Calculation and Measured neutron spectra at position 10 – ENDF/B-VI.6

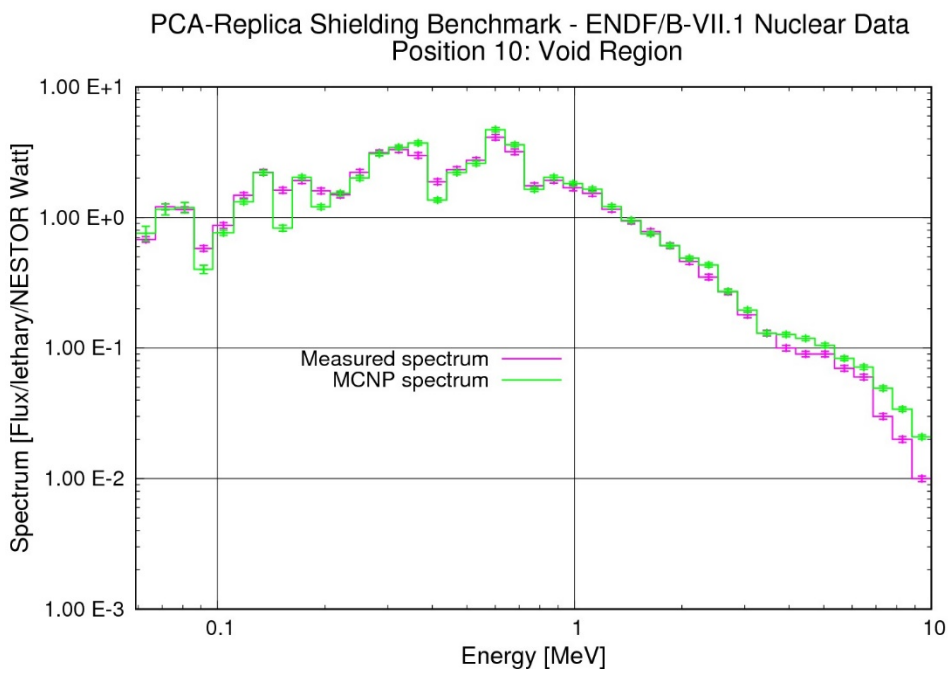

Figure S.V.2. Calculation and Measured neutron spectra at position 10 – ENDF/B-VII.1

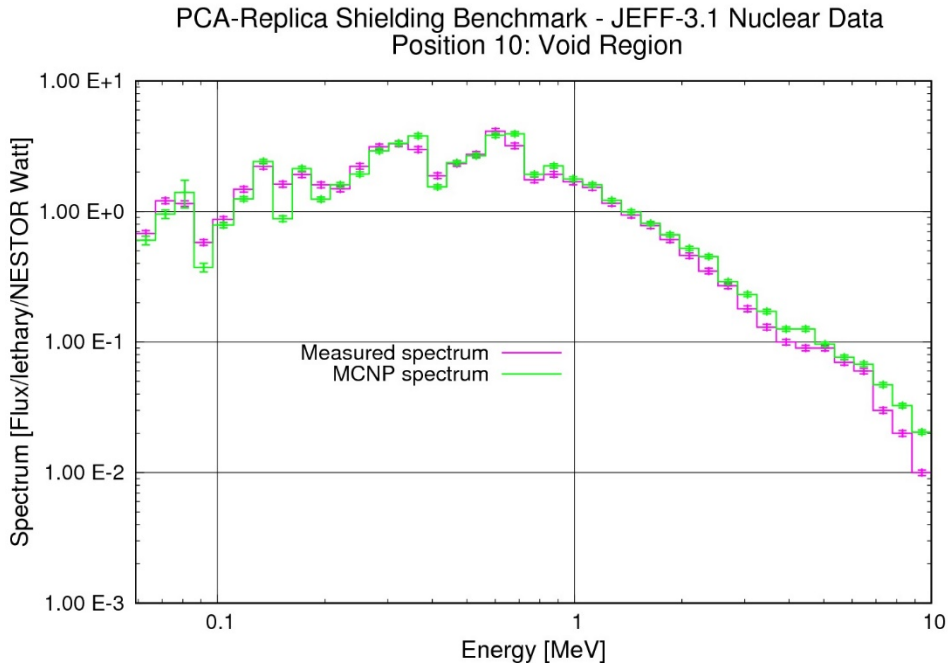

Figure S.V.3. Calculation and Measured neutron spectra at position 10 – JEFF-3.1

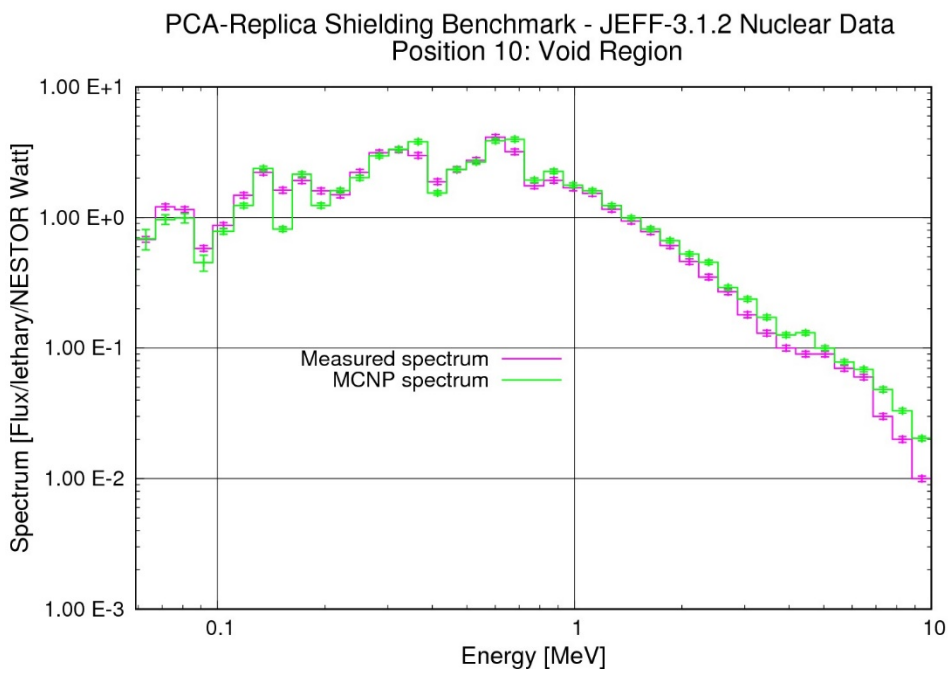

Figure S.V.4. Calculation and Measured neutron spectra at position 10 – JEFF-3.1.2

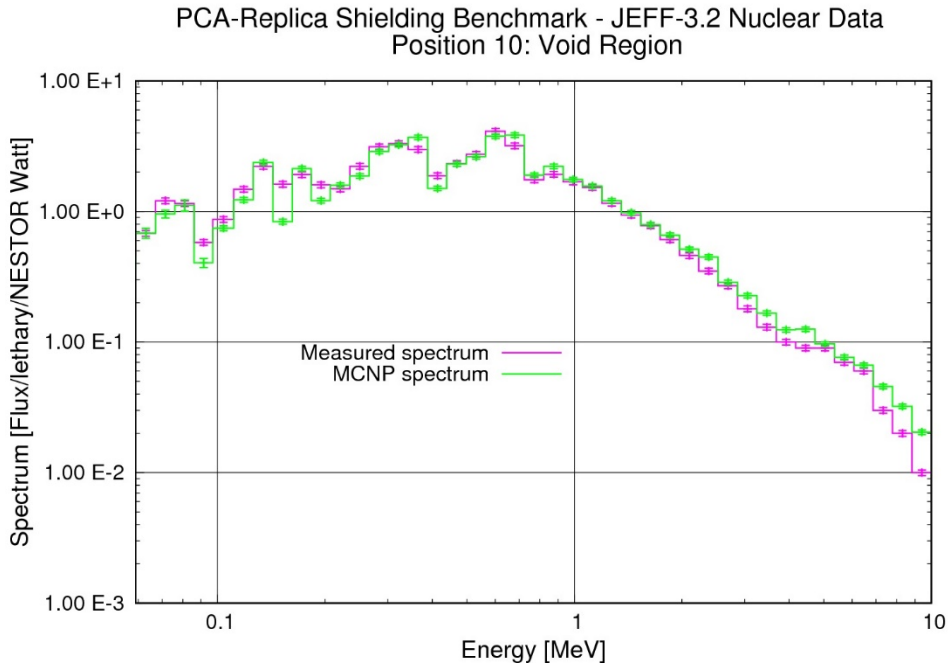

Figure S.V.5. Calculation and Measured neutron spectra at position 10 – JEFF-3.2

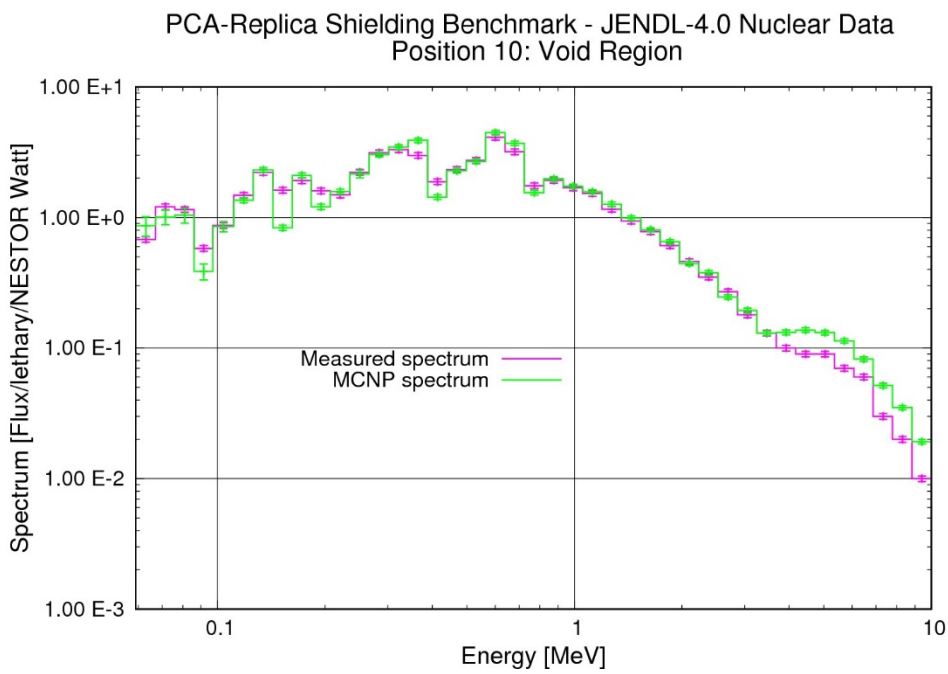

Figure S.V.6. Calculation and Measured neutron spectra at position 10 – JENDL-4.0

Again calculated and experimental values were compared in the following SR series of six Figures in which we present the (Spectrum) C/E Ratio. Figs. SR.1, SR.2, SR.3, SR.4, SR.5 and SR.6 show the C/E Spectral Ratios for both positions (PV and Void) for the ENDF-B/VI.6, ENDF/B-VII.1, JEFF-3.1,

JEFF-3.1.2, JEFF-3.2 and JENDL-4.0 transport libraries respectively. Error bars in these Figures are 1 standard deviation and include both calculation and measurement errors.

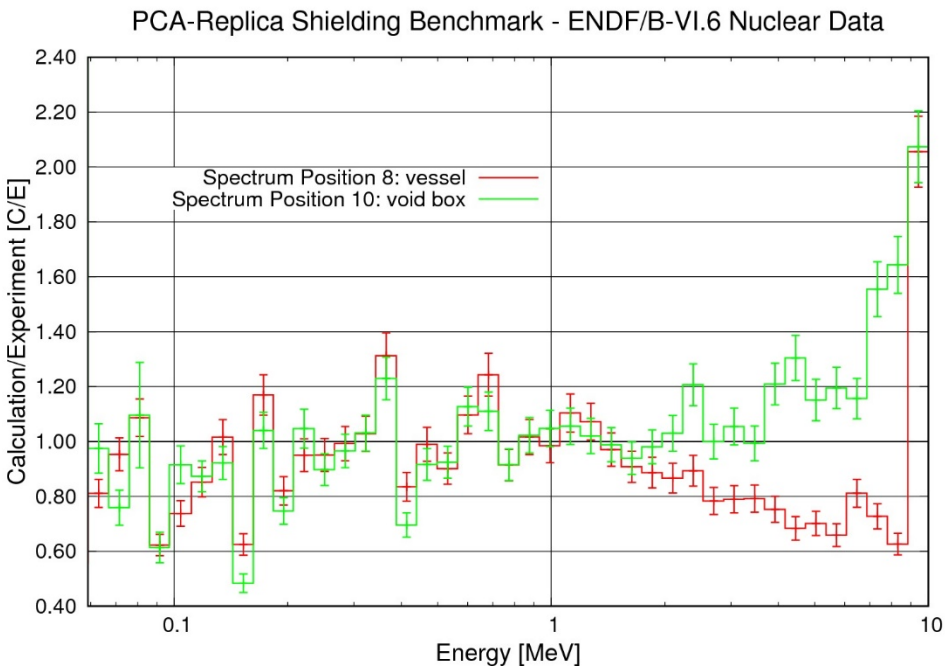

Figure SR.1. Ratio of Calculation to Experiment for neutron spectra – ENDF/B-VI.6

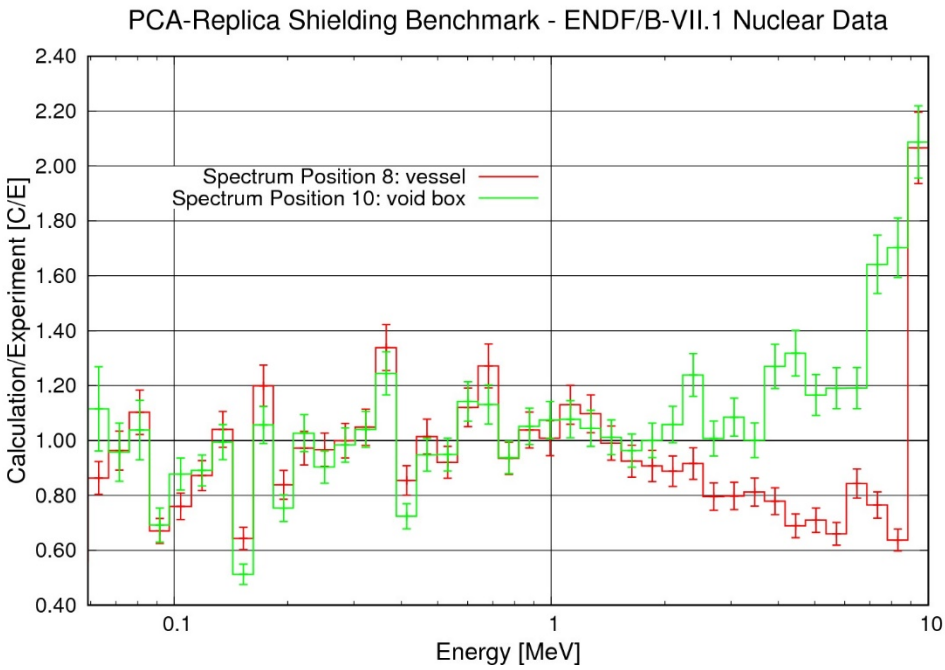

Figure SR.2. Ratio of Calculation to Experiment for neutron spectra – ENDF/B-VII.1

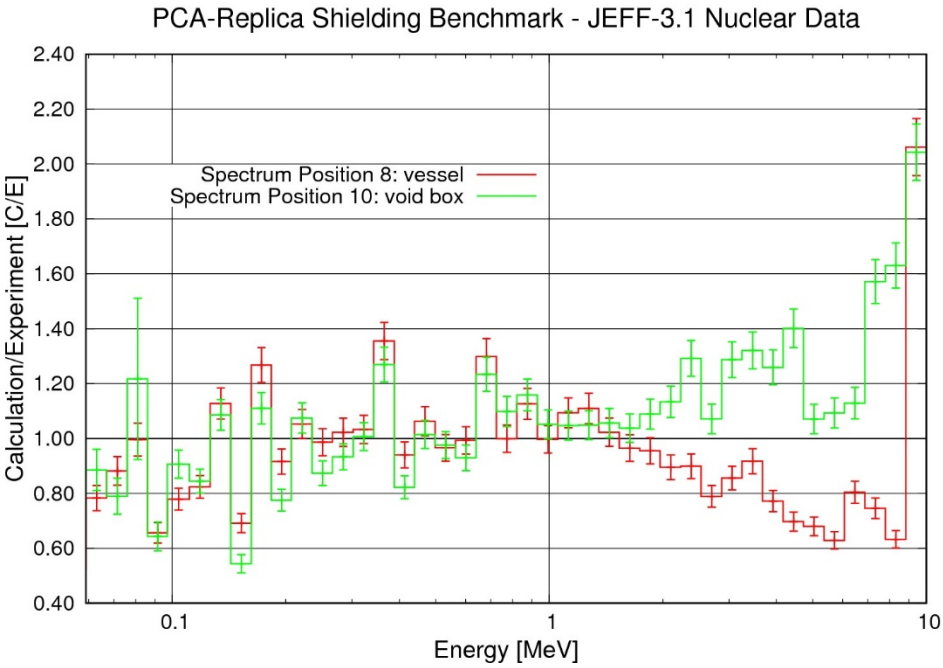

Figure SR.3. Ratio of Calculation to Experiment for neutron spectra – JEFF-3.1

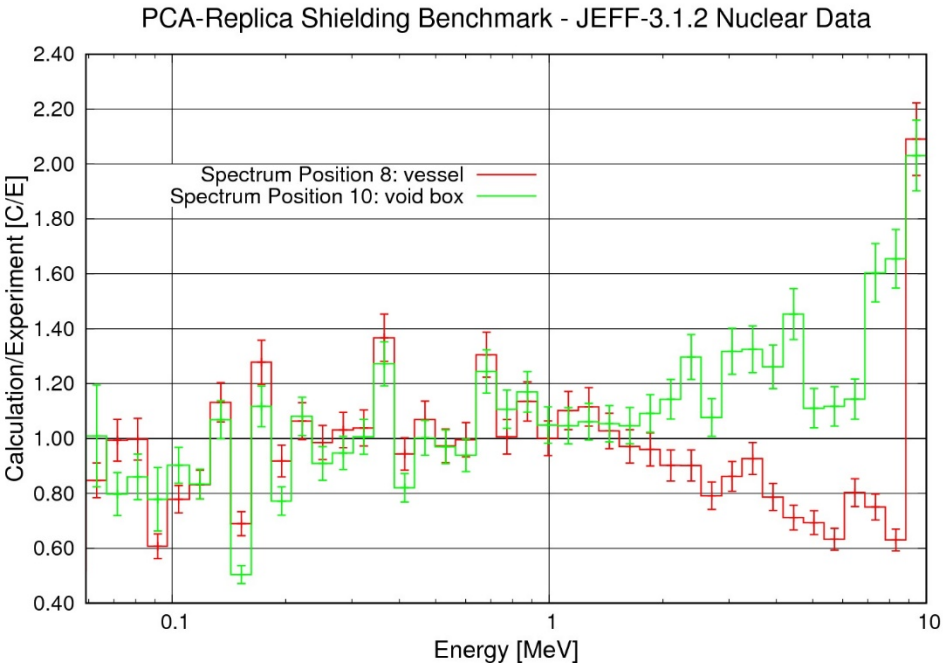

Figure SR.4. Ratio of Calculation to Experiment for neutron spectra – JEFF-3.1.2

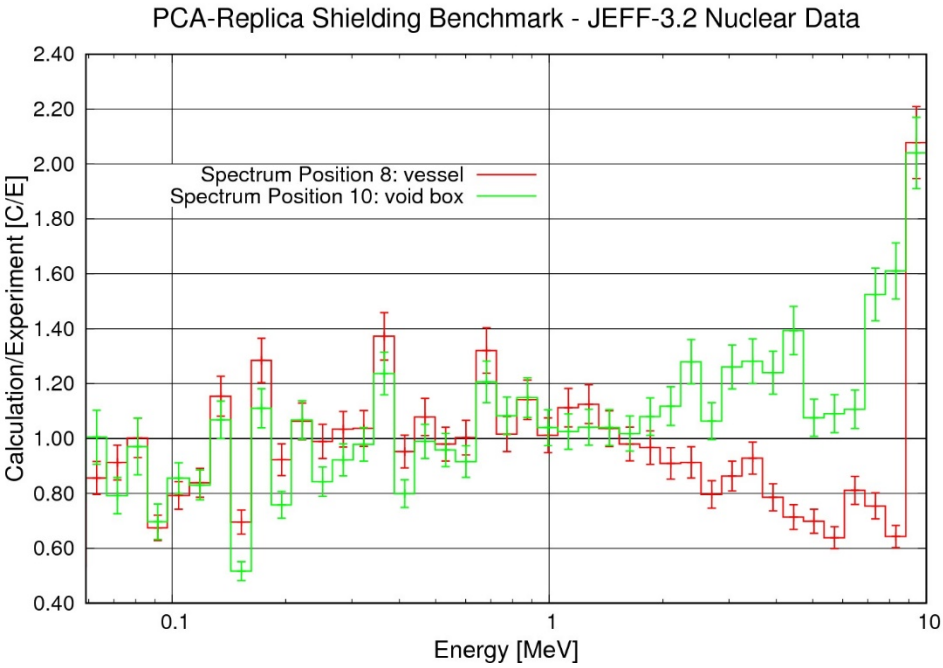

Figure SR.5. Ratio of Calculation to Experiment for neutron spectra – JEFF-3.2

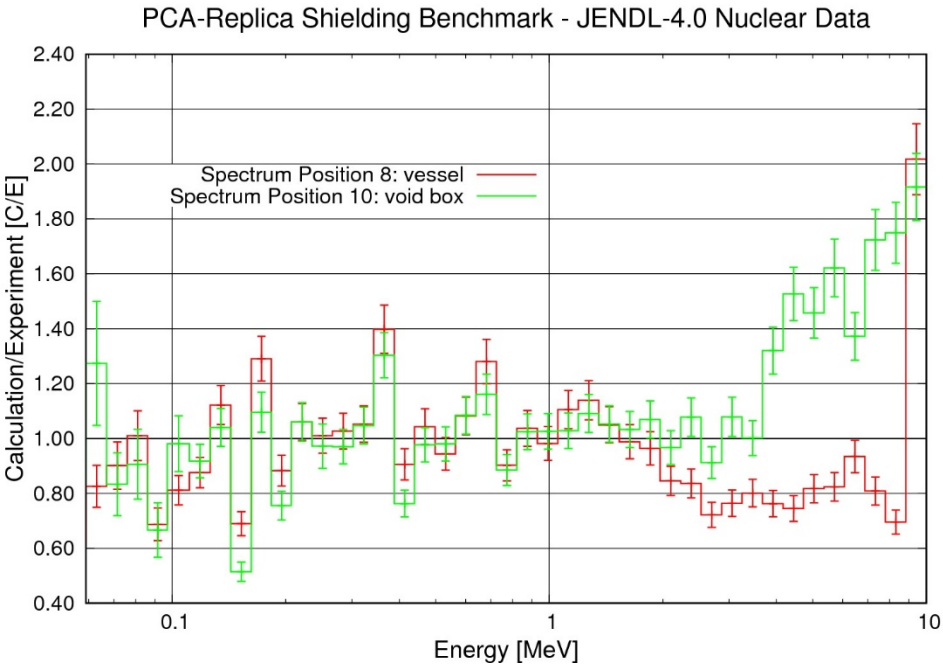

Figure SR.6. Ratio of Calculation to Experiment for neutron spectra – JENDL-4.0

4.10 Discussion

The three dosimeters, Indium, Rhodium and Sulphur, show a good agreement between calculation and measurement for the three most recent transport libraries and all five dosimeter libraries as can be seen in the D series of figures. (Furthermore the three older transport libraries show equally good agreement.) Looking more closely at the comparison by means of the C/E values in the DR series of eighteen figures:

- As far as ^{115}In(n,n')^{115m}In is concerned, the more recent IRDF dosimetry files may be slightly better than the older 532DOS file. The qualities of the six transport cross-section files are indistinguishable.
- As far as ^{103}Rh(n,n')^{103m}Rh is concerned, the qualities of the IRDF and LLLDOS dosimetry files look indistinguishable as do those of the six transport cross-section files. The calculation at the first detector position at 1.91 cm from the fission plate looks a slight overestimate. This is probably due to source modelling rather than to transport or dosimetry cross-sections.
- As far as ^{32}S(n,p)^{32}P is concerned, there is a tendency for the C/E value to increase from just below 1 to just above 1 between detector positions 8 and 10 for all dosimetry files and for all six transport files. This looks as if it could be due to the NESTOR background estimate. It is difficult to distinguish between the dosimetry files, but with regard to the transport files the two ENDF/B files may be very slightly better than any of the three JEFF files or the JENDL files.

Note that the above conclusions are extremely tentative given the 1 s.d. error bars.

Looking at the flux spectra in the series of six S.PV and six S.V Figures, we firstly note that the only uncertainties in the measurements are those of the NESTOR background. Neither the detector (hydrogen proportional counters or liquid scintillators) measurements nor the unfolding procedure (with the code RADAK) have been assigned uncertainties [8]. Therefore, the error bars on the experimental spectra are certainly underestimates.

Secondly we note at both measurement positions – in the PV and Void – in the energy range below around 1 MeV that the calculated and measured spectra fluctuate above and below each other. We may tentatively assign these differences to the unfolding procedure. Instead there remains a macroscopic effect, which is an underestimate of the calculated flux at position 8 in the PV sample above around 2 – 2.5 MeV (ignoring the very low flux in the highest energy bin 9 - 10 MeV). Such an underestimate is present for all transport files but is slightly less for JENDL-4.0. This underestimate is not present in the spectra at position 10 in the Void. On the contrary there is, if anything, a slight overestimate of the calculated flux in the same energy range. Such overestimate becomes macroscopic for JENDL-4.0 above around 3 MeV.

These effects are apparent in the six SR series of Figures where we see the C/E values. From these Figures, JENDL-4.0 looks somewhat better than the other five files at position 8 in the PV sample and somewhat worse at position 10 in the Void. The other five files look similar to each other.

4.11 Conclusions

The results show in general a good agreement with the experimental data especially for the three dosimeters. The spectra instead show calculational underestimates in the MeV energy range for the measurement within the mild steel sample and calculational overestimates in the same energy range for the measurement in the void after the mild steel sample.

4.12 Acknowledgments

The authors would like to acknowledge Dr Massimo Pescarini who supplied ~~precious~~ information in analyzing and preparing the data for the simulations and Dr Ivan Kodeli who provided useful comments on the draft text.

The computing resources and the related technical support used for the MCNP calculations have been provided by CRESCO/ENEAGRID High Performance Computing infrastructure and its staff [26]. CRESCO/ENEAGRID High Performance Computing infrastructure is funded by ENEA, the Italian National Agency for New Technologies, Energy and Sustainable Economic Development and by Italian and European research programs, see http://www.cresco.enea.it/english for further information.

4.13 References.

1. A. Ballesteros et al., “The Role of Pressure Vessel Embrittlement in the Long Term Operation of Nuclear Power Plants”, Nuclear Engineering and Design, 234 (2012) 63-68
2. A. Al Mazouzi et al., “PERFORM 60: Prediction of the Effects of Radiation for Reactor Pressure Vessel and In-core Materials Using Multiscale Modelling – 60 years Foreseen Plant Lifetime”, Nuclear Engineering and Design, 241 (2011) 3403-3415
3. S. Van Der Marck, “Benchmarking ENDF/B-VII.1, JENDL-4.0 and JEFF-3.1.1 with MCNP6”, Nuclear Data Sheets, 113 (2012) 2935-3005
4. Nicks et al., “Fission Neutron Penetration in Iron and Sodium – I. Activation Measurements”, Annals of Nuclear Energy, 15, 9 (1988) 457-469
5. Perlini et al., “Fission Neutron Penetration in Iron and Sodium – II. Neutron Spectrometry”, Annals of Nuclear Energy, 16, 4 (1989) 189-201
6. Žerovkin et al., “Re-evaluation of the EURACOS Integral Shielding Experiment Series”, Annals of Nuclear Energy, 77 (2015) 318-325
7. Nuclear Energy Agency (NEA), Shielding Integral Benchmark Archive and Database (SINBAD) section: https://www.oecd-nea.org/science/wprs/shielding/
8. Butler et al., “The PCA-Replica Experiment Part I, Winfrith Measurements and Calculations”, Reactor Physics Division, AEEW – R1736 (1984)
9. Goorley et al., “MCNP6 User’s Manual” Version 1.0, LA-CP-13-00634, Rev0 (2013)
10. Booth, “Genesis of the Weight Window and the Weight Window Generator in MCNP – A Personal History”, LA-UR-06-5807, (2006)
11. K.W. Burn, Nuclear Technology, 175-1 138-145 (2011)
12. Rose, Ed., “ENDF-201, ENDF/B-VI Summary Documentation”, BNL-NCS-17541, 4th Edition, Brookhaven National Laboratory (October 9119).
13. Chadwick et al., “ENDF/B-VII.1 Nuclear data for science and technology: cross sections, covariances, fission product yields and decay data”, Nuclear Data Sheets 112 (2011), 2887-2996
14. The JEFF-3.1 Nuclear Data Library, JEFF Report 21, OECD-NEA Data Bank, 2006

15. The JEFF-3.1.2 Nuclear Data Library, JEFF Report, OECD-NEA Data Bank: http://www.oecd-nea.org/dbforms/data/eva/evatapes/jeff_31/JEFF312/
16. The JEFF-3.2 Nuclear Data Library, JEFF-3.2 evaluated data library - Neutron data: http://www.oecd-nea.org/dbforms/data/eva/evatapes/jeff_32/
17. Shibata et al., "JENDL-4.0: A new library for nuclear science and engineering", Journal of Nuclear Science and Technology, 48(1), 1-30 (2011)
18. Little et al., "Dosimetry/Activation Cross Sections for MCNP", MS B226, (1984)
19. International Reactor Dosimetry File: IRDF-2002 – A Data Development Project of the IAEA Nuclear Data Section: https://www-nds.iaea.org/irdf2002/index.htmlx
20. International Reactor Dosimetry and Fusion File IRDFF v.1.05 – Nuclear Data Section: https://www-nds.iaea.org/IRDFF/
21. Matijević et al., "Modeling of the ORNL PCA Benchmark Using SCALE6.0 Hybrid Deterministic-Stochastic Methodology", Science and Technology of Nuclear Installations, article ID 252140 (2013)
22. Pescarini et al., "Validation of the BUGJEFF311.BOLIB, BUGENDF70.BOLIB and BUGLE-96 Cross Section Libraries on the PCA-Replica (Water/Iron) Neutron Shielding Benchmark Experiment", ENEA Report ADPFISS-LP1-024, (2014)
23. M. Pescarini, R. Orsi, M. Frisoni, "Three-Dimensional (X,Y,Z) Deterministic Analysis of the PCA-Replica Neutron Shielding Benchmark Experiment Using TORT-3.2 Code and Group Cross Section Libraries for LWR Shielding and Pressure Vessel Dosimetry, Proceedings of the 15th International Symposium on Reactor Dosimetry (ISRD-15), Paris, France, May 18-23, 2014. ENEA-Bologna Technical Report UTFISSM-P9H6-011, October 2, 2014
24. M. Pescarini, R. Orsi, M. Frisoni, "PCA-Replica (H_2O/Fe) Neutron Shielding Benchmark Experiment – Deterministic Analysis in Cartesian (X,Y,Z) Geometry Using BUGENDF70.BOLIB and BUGLE-96 Cross Section Libraries, ENEA-Bologna Technical Report UTFISSM-P9H6-009, November 20, 2014
25. Nuclear Data Service, Lund/LBNL. Table of Isotopes: http://nucleardata.nuclear.lu.se/toi/
26. G. Ponti et al., "The role of medium size facilities in the HPC ecosystem: the case of the new CRESCO4 cluster integrated in the ENEAGRID infrastructure", Proceedings of the 2014 International Conference on High Performance Computing and Simulation, HPCS 2014, art. no. 6903807, 1030-1033;